iScience

CellPress
OPEN ACCESS

Article

Identification of VIMP as a gene inhibiting cytokine production in human CD4+ effector T cells

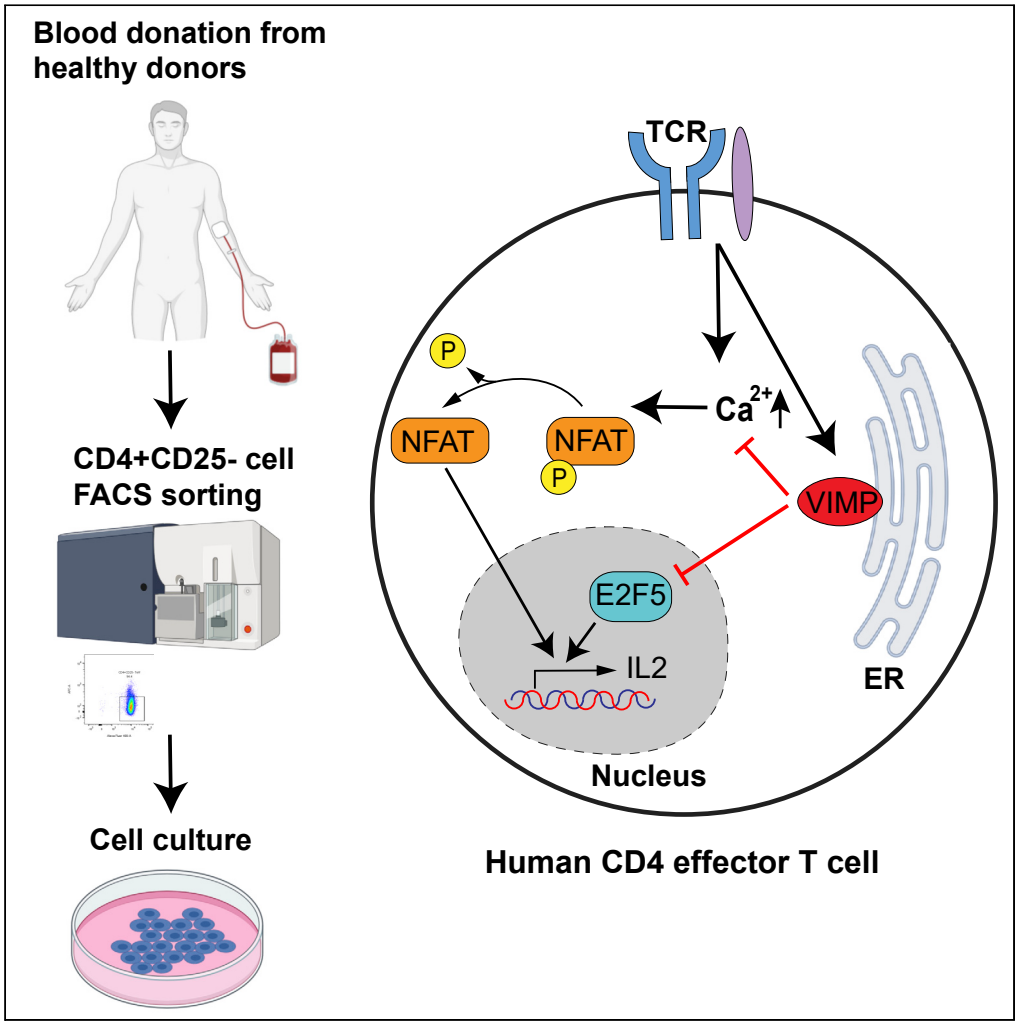

Christophe M. Capelle, Ni Zeng, Egle Danileviciute, Sabrina Freitas Rodrigues, Markus Ollert, Rudi Balling, Feng Q. He

feng.he@lih.lu

Highlights

VIMP is temporally upregulated after TCR stimulation in human CD4 effector T cells

VIMP inhibits cytokine expression in human CD4 effector T cells

VIMP inhibits cytokine expression via the NFATC2/Ca^{2+} signaling pathway

VIMP inhibits cytokine expression by controlling E2F5 expression

Capelle et al., iScience 24, 102289
April 23, 2021
https://doi.org/10.1016/j.isci.2021.102289

iScience

CellPress
OPEN ACCESS

Article

Identification of VIMP as a gene inhibiting cytokine production in human CD4+ effector T cells

Christophe M. Capelle,[1,2] Ni Zeng,[1] Egle Danileviciute,[1,3] Sabrina Freitas Rodrigues,[3] Markus Ollert,[1,4] Rudi Balling,[3] and Feng Q. He[1,3,5,6,*]

SUMMARY

Many players regulating the CD4$^+$ T cell-mediated inflammatory response have already been identified. However, the critical nodes that constitute the regulatory and signaling networks underlying CD4 T cell responses are still missing. Using a correlation-network-guided approach, here we identified *VIMP* (VCP-interacting membrane protein), one of the 25 genes encoding selenoproteins in humans, as a gene regulating the effector functions of human CD4 T cells, especially production of several cytokines including IL2 and CSF2. We identified VIMP as an endogenous inhibitor of cytokine production in CD4 effector T cells via both the E2F5 transcription regulatory pathway and the Ca^{2+}/NFATC2 signaling pathway. Our work not only indicates that VIMP might be a promising therapeutic target for various inflammation-associated diseases but also shows that our network-guided approach can significantly aid in predicting new functions of the genes of interest.

INTRODUCTION

CD4$^+$ T cells represent a major subset of immune cells that are crucial for mounting and regulating an adequate immune response. However, during many infectious and complex chronic diseases, those T cells are dysregulated, either having an impaired responsive capacity or causing adverse effects through self-recognition and/or overactivation. Therefore, rebalancing the CD4$^+$ T cell-mediated inflammatory response has been essential for the design of therapeutic options for those diseases (Zhu and Paul, 2010a). Although many players regulating the inflammatory response, cytokine production, and differentiation of CD4$^+$ T cells have already been identified in the past (Brownlie and Zamoyska, 2013; Rodriguez-Jorge et al., 2019; Saez-Rodriguez et al., 2007; Zhu and Paul, 2010b), a thorough understanding of the regulatory and signaling networks governing inflammatory cytokine production in T cells is still missing. The gap is not only attributable to the long-standing nature of traditional trial-and-error experimental procedures but also to the lack of reliable high-throughput computational prediction.

VIMP, also known as NCBI: Selenoprotein S (SELS), SELENOS, TANIS, or SEPS1, is one of the only 25 genes encoding the 21st amino acid selenocysteine in humans (Schomburg, 2011). Located in the endoplasmic reticulum (ER) membrane, VIMP is mainly known as an important component of the ER-associated degradation (ERAD) complex (Kim et al., 2007; Qin et al., 2016) and physically binds to several ER membrane proteins (Lee et al., 2015; Ye et al., 2005). VIMP plays a role in mediating retro-translocation of misfolded proteins from the ER lumen to the cytosol, where the ubiquitin-dependent proteasomal degradation takes place (Ye et al., 2004). Genome-wide association studies have shown that polymorphisms in the promoter region of *VIMP* are linked to a wide spectrum of common complex diseases, including cardiovascular disease (Alanne et al., 2007), diabetes (Karlsson et al., 2004; Olsson et al., 2011), cancer (Meplan et al., 2010; Shibata et al., 2009; Sutherland et al., 2010), sepsis (He et al., 2014), and autoimmune diseases (Santos et al., 2014; Seiderer et al., 2007), in which activation of the immune system is believed to be dysregulated (Kuchroo et al., 2012).

Meanwhile, dysfunction of the ER and the unfolded protein response causes intestinal inflammatory diseases in several murine models (McGuckin et al., 2010). Additionally, a reduced expression of VIMP causes an increased expression of inflammatory cytokines, such as NCBI: IL6, IL1β, and TNFα in macrophages

[1]Department of Infection and Immunity, Luxembourg Institute of Health (LIH), 29, rue Henri Koch, 4354 Esch-sur-Alzette, Luxembourg

[2]Faculty of Science, Technology and Medicine, University of Luxembourg, 2, avenue de Université, 4365 Esch-sur-Alzette, Luxembourg

[3]Luxembourg Centre for Systems Biomedicine (LCSB), University of Luxembourg, 6, avenue du Swing, 4367 Belvaux, Luxembourg

[4]Department of Dermatology and Allergy Center, Odense Research Center for Anaphylaxis (ORCA), University of Southern Denmark, Odense, 5000 C, Denmark

[5]Institute of Medical Microbiology, University Hospital Essen, University of Duisburg-Essen, 45122 Essen, Germany

[6]Lead contact

*Correspondence: feng.he@lih.lu

https://doi.org/10.1016/j.isci.2021.102289

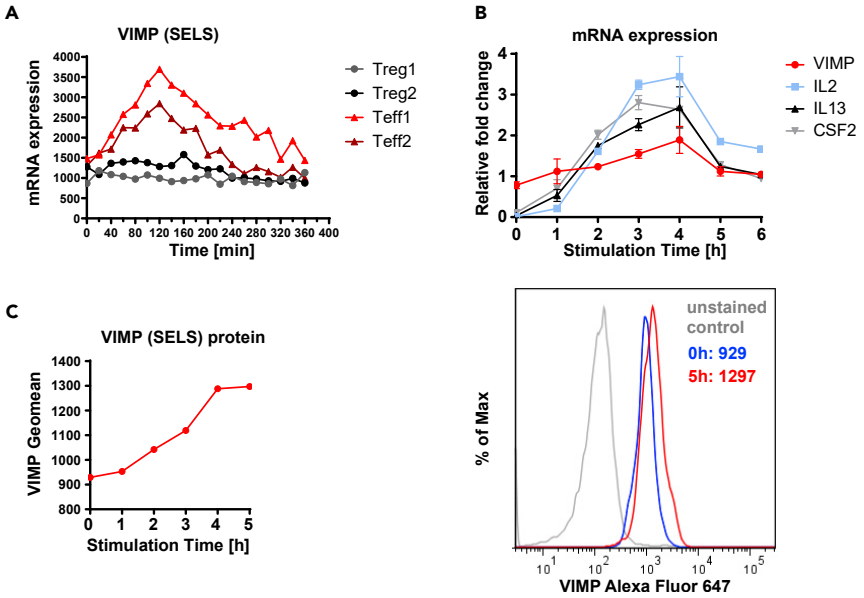

Figure 1. VIMP is temporally upregulated in Teffs following TCR stimulation

(A) The kinetics of transcriptional expression of VIMP in the first 6 h following anti-CD3/-CD28 stimulation assessed by HTR time-series microarray data. Teff1 and Teff2 are the two independent repeated HTR time-series experiments from different donors.

(B) Representative experiments, reproduced in 4 independent donors showing mRNA expression of *VIMP*, *IL2*, *IL13*, and *CSF2* measured by qPCR in Teffs stimulated by anti-CD3/-CD28 beads. The data represent the gene expression normalized to *RPS9*. Data are mean ± standard deviation (SD).

(C) Representative flow cytometry quantitative analysis showing elevation of VIMP protein expression in Teffs following TCR stimulation. Results represent four (B) and three (C) independent experiments of different donors.

(Curran et al., 2005), as well as IL1β and IL6 expression in astrocytes (Fradejas et al., 2011). However, other studies did not show significant association between *VIMP* and the examined human inflammatory diseases (Martinez et al., 2008). This controversy underlines the necessity for a better understanding of how *VIMP* contributes to the pathogenesis of some inflammatory diseases, i.e., through which cell types and which molecular pathways *VIMP* contributes to the observed dysregulated inflammatory responses. Therefore, we sought to investigate whether and how *VIMP* plays a role in relevant specific immune cells, e.g., $CD4^+$ T cells, a key subset of immune cells orchestrating different types of immune responses and being heavily involved in different complex diseases, as well as infectious diseases, such as COVID-19 (Braun et al., 2020; Mathew et al., 2020).

We have previously developed a correlation-network-guided approach, based on the guilt-by-association theory (Beyer et al., 2007; Gillis and Pavlidis, 2011; Oliver, 2000), to predict novel key genes of a given biological process or function and have successfully applied it to human $CD4^+CD25^{high}CD127^{low}$ regulatory T cells (Tregs) (Danileviciute et al., 2019; He et al., 2012). Here, we extended the strategy to human $CD4^+$ effector T cells (Teffs) that were derived and expanded from sorted $CD4^+CD25^-$ T cells by co-culturing with EBV-transformed B cells and were able to predict that VIMP might play an important role in regulating the effector responses of Teffs. Combining both the network analysis and experimental verification, we identify VIMP as a previously unreported vital endogenous inhibitor of cytokine production in human $CD4^+$ Teffs and reveal the molecular mechanisms through which VIMP regulates $CD4^+$ Teff responses.

RESULTS

VIMP is temporally upregulated following TCR stimulation in Teffs

Using our previously reported high-time-resolution (HTR) time-series transcriptome data of Tregs and Teffs following TCR (T cell receptor) stimulation in the first 6 h (He et al., 2012), we observed that the transcript level of VIMP in Teffs temporally peaked within 2–3 h following stimulation, which was followed by a gradual decrease (Figure 1A). In contrast, the *VIMP* mRNA level was kept almost constant in Tregs during the first 6 h

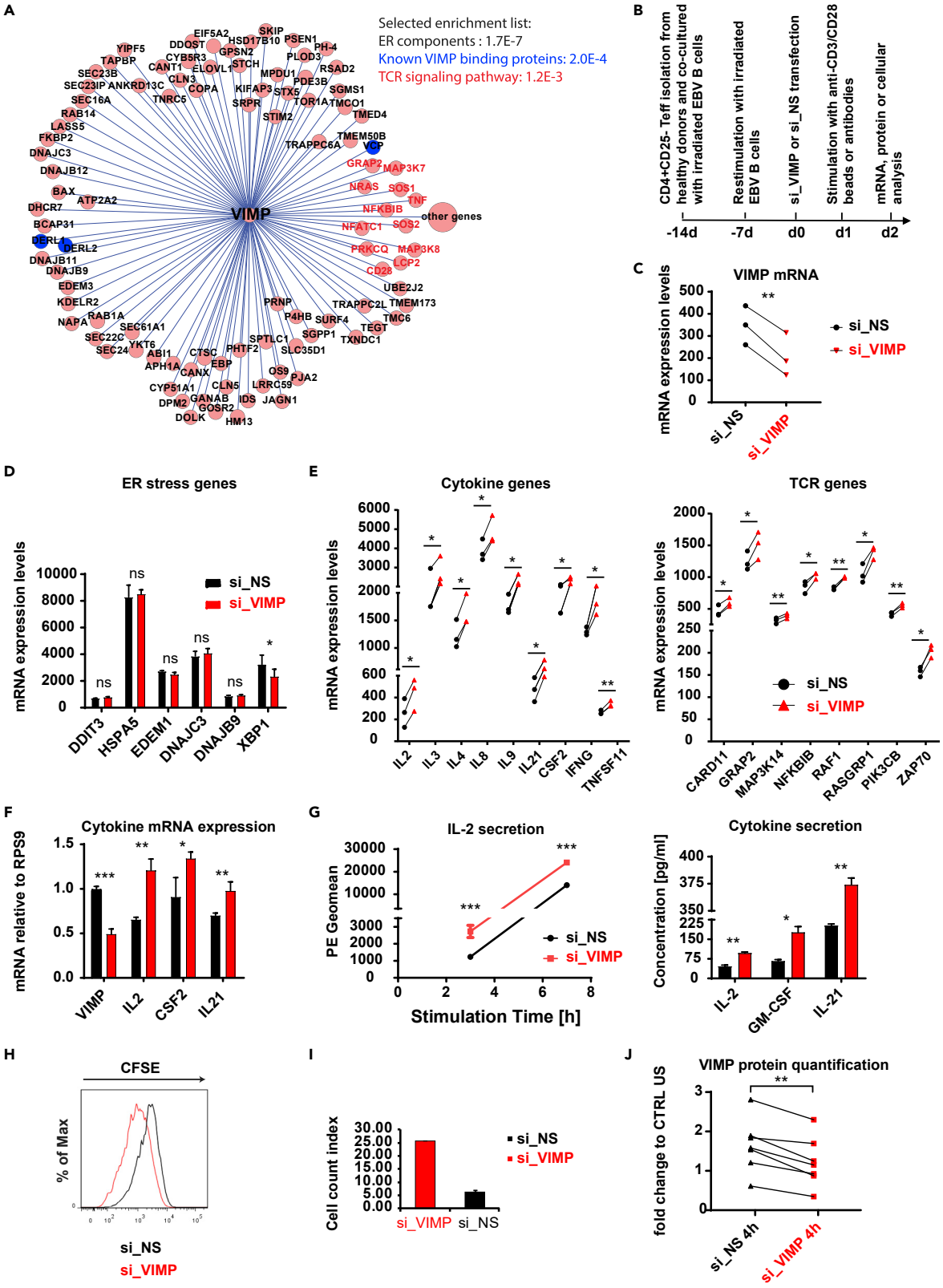
A
Selected enrichment list:
ER components : 1.7E-7
Known VIMP binding proteins: 2.0E-4
TCR signaling pathway: 1.2E-3
VIMP
other genes
B
CD4+CD25- Teff isolation from healthy donors and co-cultured with irradiated EBV B cells
Restimulation with irradiated EBV B cells
si_VIMP or si_NS transfection
Stimulation with anti-CD3/CD28 beads or antibodies
mRNA, protein or cellular analysis
-14d
-7d
d0
d1
d2
C
VIMP mRNA
mRNA expression levels
si_NS
si_VIMP
D
ER stress genes
mRNA expression levels
DDIT3
HSPA5
EDEM1
DNAJC3
DNAJB9
XBP1
E
Cytokine genes
TCR genes
IL2
IL3
IL4
IL8
IL9
IL21
CSF2
IFNG
TNFSF11
CARD11
GRAP2
MAP3K14
NFKBIB
RAF1
RASGRP1
PIK3CB
ZAP70
F
Cytokine mRNA expression
mRNA relative to RPS9
VIMP
IL2
CSF2
IL21
G
IL-2 secretion
PE Geomean
Stimulation Time [h]
Cytokine secretion
Concentration [pg/ml]
IL-2
GM-CSF
IL-21
H
CFSE
% of Max
I
Cell count index
J
VIMP protein quantification
fold change to CTRL US
si_NS 4h
si_VIMP 4h

Figure 2. VIMP controls cytokine expression in Teffs and interferes with the TCR signaling pathway

(A) The *VIMP* subnetwork extracted from the constructed Teff correlation network based on the HTR transcription microarray data. Each circle represents one gene. Each line between *VIMP* and the other genes represents a correlation link. The selected list of significantly enriched pathways or components is displayed (the p value resulted by cumulative binomial distribution test was provided for each item).

(B) Schematic of the experimental flow for the stimulation, gene silencing, and analysis of Teffs.

(C) mRNA expression showing the significant knockdown of VIMP in the microarray experiment.

(D and E) Microarray data showing the fold change or expression values in the mRNA of ER-stress responsive genes (D) and cytokine and TCR signaling genes (E). We only presented the transcripts with p values lower than 0.05 by both PLIER and RMA methods and at least a 1.2-fold change in all 3 independent donors (for details, see methods).

(F) mRNA expression measured by qPCR of the genes *VIMP*, *IL2*, *CSF2*, and *IL21* of Teffs following TCR stimulation and knockdown with either control non-specific scrambled siRNA (si_NS) or *VIMP*-specific siRNA (si_VIMP). Before stimulation, the cells were first transfected with siRNA for 1 day (for all the figures).

(G) The concentration of the cytokines IL2, GM-CSF, and IL21 detected in the cell culture medium following anti-CD3/-CD28 stimulation for different time points (left panel, IL2 alone by CBA measurement) or 8 h (right panel, multiplexing by MSD). PE geometric mean (Geomean) corresponds to the IL2 concentration signal in the media.

(H and I) Proliferation of Teffs following VIMP knockdown and TCR stimulation, measured by CFSE proliferation assay (H) and by counting the T cells following stimulation (I). Before Teffs were co-cultured with EBV-transformed B cells for 2 days, they were first transfected with siRNA for 1 day.

(J) Quantification of the western blot protein bands and normalization of VIMP to the housekeeping gene GAPDH. Each dot represents one sample. CTRL US, unstimulated Teffs treated with si_NS. Data are mean ± SD. The p values are determined by a two-tailed paired Student's t test (except for A and G). The results in (G) were analyzed using non-paired t test. ns or unlabeled, non-significant; *p<=0.05, **p<=0.01, and ***p<=0.001. Results represent three (C–E) and six (F–J) independent experiments of different donors. See also Figure S1.

following TCR stimulation (Figure 1A), indicating a possible specific role for VIMP in Teffs. Our quantitative real-time PCR (qPCR) results validated the transitionally elevated expression of the VIMP transcript in Teffs isolated from different healthy donors (Figure 1B). We also observed a correlation over time between the transcription levels of NCBI: *VIMP*, *IL2*, *IL13,* and *CSF2* (GM-CSF) following TCR stimulation, indicating a potential regulatory relationship between *VIMP* and some of the cytokines in Teffs (Figure 1B). By flow cytometry (Figure 1C), we confirmed the gradual upregulation of VIMP protein expression in the first 5 h following TCR stimulation. In summary, both mRNA and protein expression of VIMP were upregulated following TCR stimulation, which was correlated with the expression of several examined cytokines, indicating a potential role of VIMP in regulating Teff responses.

VIMP inhibition upregulates cytokine expression in Teffs

The upregulation of VIMP and its correlation to cytokine expression encouraged us to further investigate VIMP's potential role in CD4 T cell responses. We and others have previously shown that the enriched pathways, processes or functions among the genes surrounding a given hub gene in the correlation network might give valuable indications on potential new functions of the given hub gene (Danileviciute et al., 2019; He et al., 2012). Therefore, we used our correlation network-guided approach to predict the potential functions of *VIMP* by identifying the enriched pathways among the genes that are linked to *VIMP* within the subnetwork of the Teff correlation network, which was extracted from our published HTR datasets and networks (He et al., 2012) (Figure 2A).

Consistent with its known function and its localization in the ER membrane, the genes surrounding *VIMP* in the correlation network were significantly enriched for ER components (p value = 1.7×10^{-7}, cumulative binomial distribution) (Figure 2A). Furthermore, 3 of the 10 experimentally validated VIMP-binding partners found in the literature in other cellular types are directly linked to *VIMP* in the Teff correlation network (p value = 2.0×10^{-4}, http://string-db.org [Szklarczyk et al., 2019]), indicating the reliability of our method. Surprisingly, the pathway enrichment analysis shows that the genes linked to *VIMP* are significantly enriched for components involved in the TCR signaling pathway (p value = 1.2×10^{-3}, cumulative binomial distribution) (Figure 2A), suggesting a potential role of VIMP in the Teff response according to our network-based analysis strategy (Danileviciute et al., 2019; He et al., 2012). However, the genes linked to the hub gene of interests in the correlation network could follow at least two scenarios (He and Ollert, 2016; Langfelder and Horvath, 2008; van Dam et al., 2018). First, those genes could be co-regulated by chance with the hub gene and perform independent functions. Second, those genes could be co-expressed with the hub gene and play related roles in the same pathways to coordinate cellular resources for a particular function or purpose under certain conditions. We will test these possibilities in this work.

To systematically assess whether and how *VIMP* controls the inflammatory response of Teffs, we performed a transcriptome analysis of CD4 Teffs isolated from peripheral blood mononuclear cells (PBMCs) of three healthy donors that were subjected to a specific-small interfering RNA (siRNA) knockdown of VIMP

(si_VIMP) or a control unspecific scrambled siRNA (si_NS) followed by anti-CD3/-CD28 stimulation (Figure 2B). As shown in Figure 2C, the mRNA expression of *VIMP* was significantly downregulated in Teffs by using siRNA knockdown.

As VIMP has reported functions in ER stress, we first checked the ER-stress responsive genes in the transcriptomic data of the Teffs transfected with si_VIMP versus that treated with control siRNA (si_NS). By perturbing the expression of *VIMP*, we expected a change in the expression of some ER-stress responsive genes. Nonetheless, our transcriptome data of Teffs with VIMP partial knockdown did not show any significant change in mRNA expression of those genes (e.g., NCBI: *CHOP [DDIT3]*, *GRP78 [HSPA5]*, *EDEM1*, *DNAJC3 [P58IPK]*, and *DNAJB9 [ERdj4]* [Lee et al., 2003]) (Figure 2D). Only the expression of the ER-stress regulator *XBP1* (Yoshida et al., 2001) was significantly but modestly decreased. Indeed, data from intestinal epithelial cells show that VIMP is only a marker, but not a regulator, of ER stress (Speckmann et al., 2014). This shows that the direct involvement of VIMP in ER stress might not be ubiquitous to all cell types. We therefore ruled out the possibility that VIMP directly regulates the expression of the ER-stress responsive genes, indicating other roles of VIMP in modulating the Teff responses.

Considering that the TCR signaling pathways were significantly enriched in the VIMP correlation network, we further analyzed the genes related to the TCR signaling pathway in Teffs after *VIMP* knockdown. Notably, we found 13 significantly upregulated genes involved in the TCR signaling, including several cytokines, namely, NCBI: *IL2*, *IL4*, *CSF2*, and *IFNG* (refer to https://www.genome.jp/kegg-bin/show_pathway?hsa04660) in the microarray datasets of the Teffs, although only subjected to a partial knockdown of *VIMP* (Figure 2E). Moreover, transcripts of the key TCR-related signaling molecules, such as NCBI: *GRAP2*, *ZAP70*, *RASGRP1*, and *RAF1*, were significantly affected (Figure 2E). With the observation in mind that *VIMP* and the TCR signaling-related genes were directly linked in our HTR correlation network (Figure 2A), this effect of the siRNA perturbation was not unexpected. Our results suggest that VIMP negatively regulates the expression of specific cytokines and influences the expression of important components of the TCR signaling pathway.

To further confirm whether *VIMP* regulates cytokine expression in Teffs, using PBMC of independent donors we measured the cytokine mRNA expression by qPCR and the secreted cytokines of Teffs that were exposed to a *VIMP* knockdown. Indeed, NCBI: *IL2*, *IL21*, and *CSF2* mRNA were significantly upregulated in stimulated Teffs transfected with si_VIMP, compared with control Teffs (with si_NS) (Figure 2F). This observation was further consolidated by increased IL2, IL21, and GM-CSF protein levels in the culture media of stimulated Teffs transfected with si_VIMP, compared with that treated with control scrambled siRNA (Figure 2G). Furthermore, the VIMP knockdown also significantly promoted T cell proliferation as indicated by both carboxyfluorescein succinimidyl ester (CFSE) peak shifting and Teff cell number counting experiments (Figure 2H and 2I). As IL2 concentration was already significantly higher at 3 h following stimulation (Figure 2G) and no cell division was expected, the enhanced IL2 secretion following VIMP knockdown was not simply caused by more Teffs. All the analyses were done under the precondition that VIMP protein was successfully silenced (Figure 2J). In short, VIMP negatively regulates the expression of several cytokines in Teffs following stimulation.

Considering that *VIMP* encodes selenocysteine, thus requiring selenium (Se) for its protein synthesis, and the fact that a relatively low concentration of Se was used in our T cell media (IMDM, ~0.066 μM), we next supplemented sodium selenite in the T-cell culture media to the range of physiological concentrations (~1 μM) (Rauhamaa et al., 2008; Safaralizadeh et al., 2005; Stranges et al., 2011). In line with the reported inverse association between Se status and inflammatory bowel diseases (Kudva et al., 2015), increasing the concentration of Se in the media generated a dose-dependent suppressive effect on IL2 production of sorted CD4 Teffs following TCR stimulation (Figures S1A and S1B). Meanwhile, increasing Se concentration to a physiological concentration upregulated the VIMP expression of stimulated CD4 Teffs in three of five tested donors (Figures S1C and S1D). These results again indicate that Se, at least partially, negatively regulates the expression of cytokines, e.g., IL2 in CD4 Teffs via VIMP, which is in line with our knockdown results.

VIMP controls cytokine expression via the transcription factor E2F5

Next, we aimed to identify any (co-)transcription factors (TFs), whose expression were significantly affected after silencing VIMP, as they often serve as the key components orchestrating the activity of the relevant pathways. Through a systematic analysis of all the known mammalian TFs or co-factors (Zhang et al., 2012) in our microarray

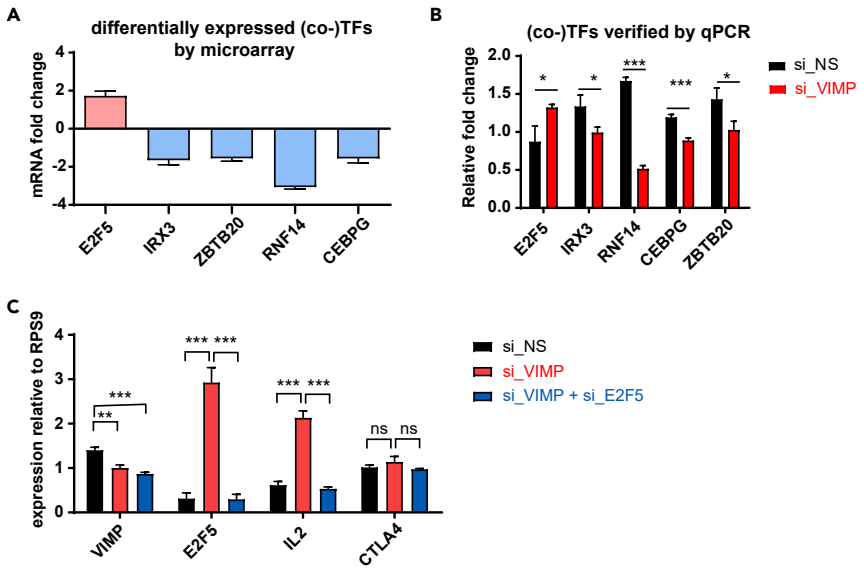

Figure 3. VIMP inhibits E2F5 to regulate IL2 expression

(A) The most significantly affected (co-)transcription factors selected from our microarray analysis including three donors; the y axis indicates the fold change between Teffs transfected with siRNA specific against VIMP(si_VIMP) or non-specific scrambled si_RNA (si_NS).

(B) mRNA expression measured by qPCR from Teffs of independent healthy donors of the genes displayed in (A) to confirm the change in their expression levels following *VIMP* knockdown.

(C) mRNA expression measured by qPCR of the genes *VIMP*, *E2F5*, *IL2*, and *CTLA4* of Teffs transfected with si_NS, si_VIMP, or both si_VIMP and si_E2F5. Data are mean ± SD. The p values are determined by a two-tailed paired Student's t test. ns or unlabeled, non-significant; *p<=0.05, **p<=0.01, and ***p<=0.001. Results represent four (B and C) independent experiments of different donors.

datasets, NCBI: *E2F5* was found to be the most significantly upregulated TF, following a partial VIMP knockdown (Figure 3A). Conversely, NCBI: *RNF14* (ring finger protein 14) was the most downregulated cofactor together with the downregulated TFs NCBI: *CEBPG* (CCAAT enhancer binding protein gamma), NCBI: *ZBTB20* (zinc finger and BTB domain containing 20), and NCBI: *IRX3* (Iroquois homeobox 3) (Figure 3A). We further confirmed the expression change of these (co-)TFs by qPCR in independent healthy donors (Figure 3B).

E2F5 has been reported to be a downstream target of IL-2 in an immortalized human T cell line (Brennan et al., 1997). But to our knowledge, there are no reports yet of *E2F5* sitting at the upstream pathways regulating inflammatory responses, especially cytokine production. Nevertheless, being the most significantly upregulated TF following a partial knockdown of *VIMP*, we assumed that *E2F5* might be an important component in the regulatory pathway through which *VIMP* regulates the Teff inflammatory response.

Therefore, we decided to investigate whether *VIMP* controls the cytokine expression by negatively regulating *E2F5* expression in stimulated Teffs. To examine this hypothesis, we silenced *VIMP* alone or in combination with *E2F5* and measured the expression of selected cytokines by qPCR. In addition to the reduced expression of *VIMP*, the upregulation of *E2F5* expression that was driven by *VIMP* knockdown was abolished in the *VIMP* and *E2F5* double knockdown Teffs (Figure 3C). Silencing *VIMP* alone upregulated *IL2* expression in stimulated Teffs, whereas a dual knockdown of *VIMP* and *E2F5* suppressed the surge of *IL2* caused by VIMP knockdown alone (Figure 3C). Even though *E2F5* is a general regulator of transcription, we did not observe any effect of *E2F5* knockdown on genes that are not directly involved in Teff inflammatory response, such as NCBI: *CTLA4* (Figure 3C). This excluded a generalized effect of *E2F5* on the transcriptional regulation in Teffs. In brief, our data support the fact that *VIMP* regulates the expression of inflammatory cytokines, i.e., IL2, by restraining the expression of the TF *E2F5* in Teffs.

VIMP controls cytokine expression via the Ca^{2+}/NFATC2 signaling pathway

To further delineate VIMP's regulatory pathways beyond the altered expression of individual TFs determined by the differential expression analysis of our microarray datasets, we applied the Ingenuity Pathway Analysis (IPA) to

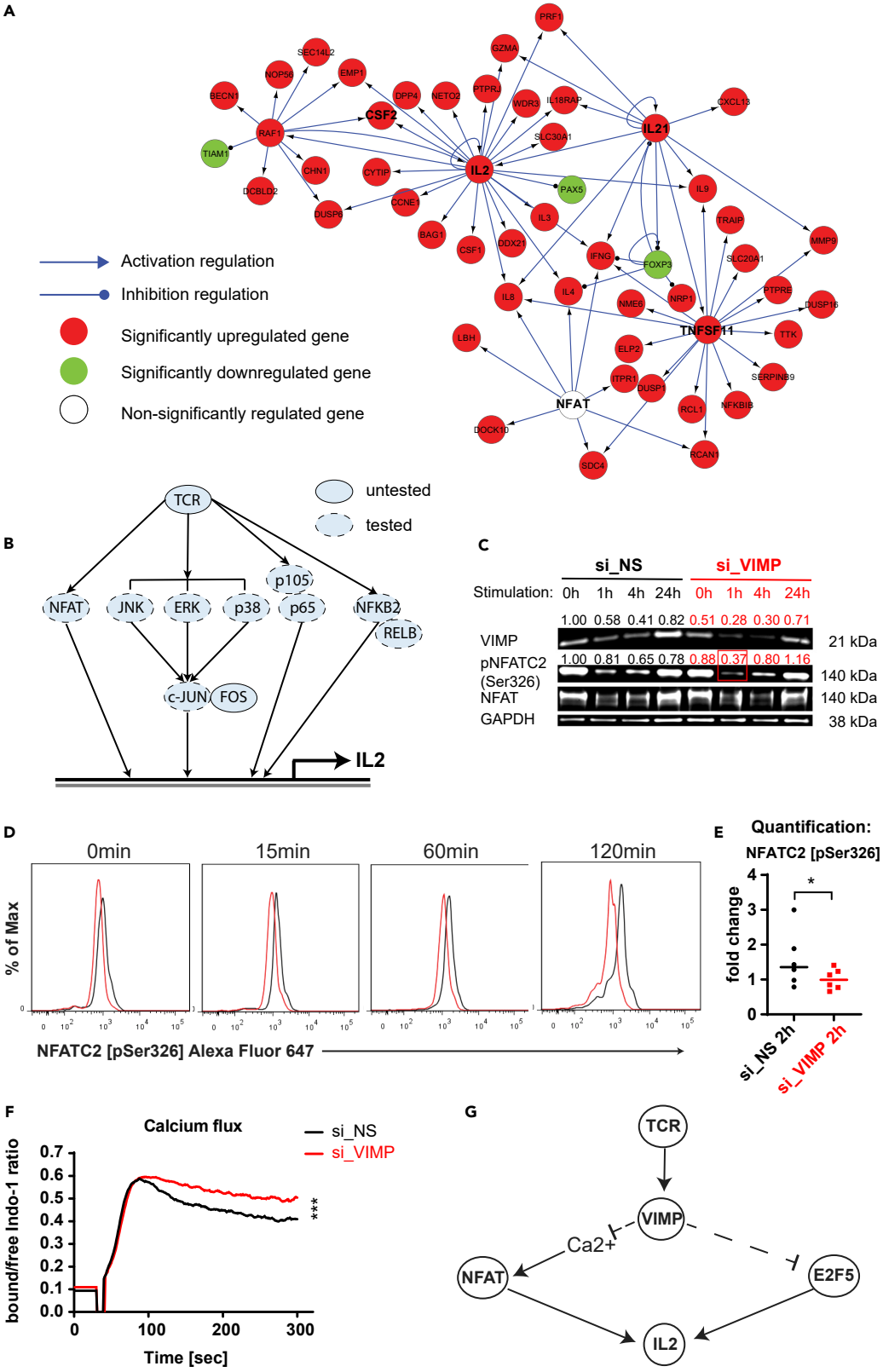
A
Activation regulation
Inhibition regulation
Significantly upregulated gene
Significantly downregulated gene
Non-significantly regulated gene
PRF1
GZMA
SEC14L2
NOP56
EMP1
BECN1
DPP4
NETO2
PTPRJ
WDR3
IL18RAP
CXCL13
CSF2
RAF1
SLC30A1
IL21
TIAM1
CHN1
CYTIP
IL2
PAX5
IL9
DCBLD2
CCNE1
DUSP6
IL3
TRAIP
MMP9
BAG1
CSF1
DDX21
IFNG
FOXP3
SLC20A1
IL8
IL4
NME6
NRP1
PTPRE
DUSP16
LBH
TNFSF11
TTK
ELP2
ITPR1
DUSP1
SERPINB9
NFAT
RCL1
NFKBIB
DOCK10
RCAN1
SDC4
B
untested
tested
TCR
p105
NFAT
JNK
ERK
p38
p65
NFKB2
RELB
c-JUN
FOS
IL2
C
si_NS
si_VIMP
Stimulation: 0h 1h 4h 24h 0h 1h 4h 24h
1.00 0.58 0.41 0.82 0.51 0.28 0.30 0.71
VIMP
21 kDa
1.00 0.81 0.65 0.78 0.88 0.37 0.80 1.16
pNFATC2 (Ser326)
140 kDa
NFAT
140 kDa
GAPDH
38 kDa
D
0min
15min
60min
120min
% of Max
NFATC2 [pSer326] Alexa Fluor 647
E
Quantification:
NFATC2 [pSer326]
fold change
si_NS 2h
si_VIMP 2h
F
Calcium flux
si_NS
si_VIMP
bound/free Indo-1 ratio
Time [sec]
G
TCR
VIMP
Ca2+
NFAT
E2F5
IL2

Figure 4. VIMP controls cytokine expression via the Ca^{2+}/NFATC2 phosphorylation pathway

(A) Network representation of the cytokine and TCR-related genes affected by the knockdown of VIMP by Ingenuity Pathway Analysis (IPA). Red, significantly upregulated genes; green, significantly downregulated genes; white, non-significantly affected gene at the transcriptional level. The link with arrow indicates a known direct or indirect positive transcription regulation; the link with circle indicates a negative one from the IPA knowledge databases.
(B) Graphical representation of the major signaling pathways downstream of the TCR signaling, (un)tested for their phosphorylation levels.
(C and D) Phosphorylation of NFATC2 (NFAT1) in Teffs assessed by western blot (C) or flow cytometry (D) at different time points following anti-CD3/-CD28 stimulation (C) or PMA/ionomycin stimulation (D). Before stimulation, Teffs were first transfected with specific siRNA against VIMP (si_VIMP) or non-specific siRNA (si_NS) for 24 h. (D) Representative flow cytometry plots of pNFATC2 in Teffs.
(E) Pooled pNFATC2 data from multiple donors at 120 min post stimulation. For (D and E), only gated viable Teffs were displayed for all the phosphorylation results. The y axis represents the percentage of maximum (scales each curve to mode = 100%) (% Max). The fold change was calculated by normalizing the geometric mean (Geomean) of the fluorescence intensities of all the conditions to that of the unstimulated control siRNA knockdown condition.
(F) Representative graph of 3 independent experiments for the calcium flux in Teffs following stimulation. The one displayed here used ionomycin stimulation after si_VIMP or si_NS transfection for 24 h. The y axis represents the ratio between calcium-bound and free Indo-1 dye over time.
(G) Graphical representation summarizing the two mechanisms through which VIMP regulates cytokine expression in CD4 Teffs. Data are mean ± SD. The p values are determined by a two-tailed paired Student's t test. ns or unlabeled, non-significant; *p<=0.05, **p<=0.01, and ***p <=0.001 . Results represent three (C and F) and six (D and E) independent experiments of different donors. See also Figures S2 and S3.

map the up- or downregulated cytokine and TCR related genes into the known regulatory network structures. We found that many of those differentially expressed genes are controlled by the expression change of the so-called hub genes NCBI: *IL2*, *RAF1*, *IL21*, and *TNFSF11*, as well as nuclear factor of activated T cells (NFAT) activity (Figure 4A). Although *NFAT* transcript expression was not significantly affected (Figure 4A), its activity was predicted to be increased by the IPA computational analysis. Meanwhile, we investigated the *VIMP* subnetwork in the Teff correlation network in more depth (Figure 2A). We found that genes for several components of NF-κB, NFAT, and MAPK signaling pathways were also directly linked to *VIMP*, indicating that those pathways might be involved in the regulation of the inflammatory response of Teffs by VIMP. To determine whether any of the relevant signaling pathways downstream of the TCR pathway that were suggested by the computational analysis are affected by VIMP expression, we quantitatively assessed the phosphorylation levels of up to 10 various signaling proteins by flow cytometry (Figure 4B). Canonical (NFKB1, p105, and p65) and non-canonical (NFKB2, p100, and RELB) NF-κB signaling pathways, as well as several MAP kinase sub-pathways (ERK1/2, p38, JNK1/2, and cJun) were not significantly affected in their phosphorylation levels (Figures S2A–S2E and S3). The phosphorylation level in one of the NFAT family members, NFATC1, was also not significantly affected by VIMP knockdown in stimulated Teffs (Figures S2F and S3). However, the phosphorylation level at the specific site Ser326 of another NFAT family member, NCBI: NFATC2 (also known as NFAT1), was significantly reduced even following a partial VIMP knockdown, as quantified by both flow cytometry and western blotting in Teffs isolated from different donors (Figures 4C–4E and S2G). Total NFAT1 protein remained unaffected by the partial VIMP knockdown (Figure S2H). In resting T cells, NFAT proteins are phosphorylated and reside in the cytoplasm (Okamura et al., 2000; Sharma et al., 2011). To be able to translocate to the nucleus and induce gene expression, NFAT is de-phosphorylated following the TCR signaling. As the NFAT activity is known to regulate IL2 expression in T cells (Chow et al., 1999), the observed downregulation of NFATC2 phosphorylation, following *VIMP* knockdown, demonstrated that the upregulation of IL2 expression was, at least in part, due to an increase in NFAT activity.

The distinguishable feature of NFAT is that it relies on Ca^{2+} influx and subsequent Ca^{2+}/calmodulin-dependent phosphatase calcineurin to become dephosphorylated and being able to translocate to the nucleus to induce gene expression (Hogan et al., 2003). Although *VIMP* has not yet been linked to the calcium signaling, other selenoproteins have been described to regulate the calcium signaling and homeostasis (Pitts and Hoffmann, 2018). We therefore further asked whether *VIMP* knockdown affects the calcium flux in Teffs and measured it by flow cytometry using the calcium indicator Indo-1. Indeed, the Teffs in which *VIMP* was silenced versus the control Teffs showed a significantly higher flux of Ca^{2+} ions (Figure 4F), further illustrating the increased NFATC2 activity and IL2 expression.

In summary, our data strongly suggest that *VIMP* inhibition upregulates the expression of cytokines, such as IL2, by two mechanisms at different levels (Figure 4G). On the transcription regulatory level, *VIMP* controls the expression of TF E2F5 and multiple genes involved in the TCR signaling and the inflammatory response. On the signaling transduction level, *VIMP* knockdown modulates Teff responses by controlling the Ca^{2+} flux and the downstream NFATC2 de-phosphorylation.

DISCUSSION

So far many important components in the regulatory or signaling networks modulating the inflammatory responses of Teffs still remain elusive. With the development of systems biomedicine, researchers have

greater opportunities to use top-down approaches to objectively infer and identify novel key genes or proteins in the process of interest.

In this work, we have applied our previously published correlation network-guided strategy to predict new genes regulating the effector functions of $CD4^+CD25^-$ Teff cells, i.e., cytokine production. We identified VIMP, encoding an ER membrane-associated selenoprotein, as a previously unrecognized negative regulatory gene of the Teff response. VIMP is best known for its critical functions in ER stress, which was demonstrated in some tested cell types. Our transcriptomic correlation network in Teffs also indicates that VIMP might be involved in ER-stress-related functions. However, as shown here, inhibiting the VIMP expression in primary human Teffs did not support the fact that VIMP is critical for the transcriptional regulation of ER-stress responsive genes in Teffs. Next, the correlation network navigated us to check the TCR signaling pathways. As demonstrated in different layers, VIMP indeed substantially regulated the expression of several inflammatory cytokines, especially IL2, in Teffs. We next investigated the VIMP regulatory mechanisms using primary human Teffs isolated from different healthy donors, the most clinically relevant available materials. Combining the analysis of time-series correlation network with knockdown-based regulatory networks, we further predicted that VIMP might go through the NFAT signaling pathway, or MAP kinase or NFKB signaling pathways to mediate the effector functions of Teffs. After testing those signaling pathways one by one, we finally pinpointed that VIMP inhibition enhances cytokine production of Teffs via the NFATC2 signaling pathway. The involvement of the NFAT signaling pathway was further backed by the influence of VIMP inhibition on calcium (Ca^{2+} influx, which is vital to the activation of the NFAT signaling pathway). Coincidently, Joost and colleagues have recently reported the co-expression of *VIMP* and *NFATC2* transcripts within the murine interfollicular epidermis using single-cell RNA sequencing analysis, indicating from another angle that our conclusion might hold true (Joost et al., 2016). We have also shown that *E2F5* plays a significant role in the VIMP-mediated regulation of the Teff IL2 expression. However, whether the *E2F5* pathway and the Ca^{2+}/NFATC2 signaling controls VIMP-mediated IL2 expression in a sequential manner or in parallel requires further investigation. Although the published association studies have already shown that the VIMP expression levels and/or SNPs are correlated with the risk of several types of diseases, it remains unsolved whether VIMP deficiency can regulate the effector functions of Teffs *in vivo*.

In our TF-focused analysis, we identified not only *E2F5* as the most upregulated TF but also several downregulated TF genes, following VIMP knockdown. Among those downregulated ones, *RNF14* (ring finger protein 14), a less characterized gene, represented the most significantly downregulated co-factor, attributable to VIMP knockdown in Teffs. Although very limited, a published report shows that *RNF14* modulates the expression of inflammatory and mitochondria-related genes in a murine myoblast cell line (Ingham et al., 2014). Another downregulated TF *ZBTB20,* originally studied in human dendritic cells (Zhang et al., 2001), and later in myeloid cells (Liu et al., 2013) and B cells (Zhu et al., 2018), has been shown to regulate their effector functions and differentiation. The Iroquois homeobox 3 (*IRX3)* has been recently linked to human CD8 T cell survival and fate determination *in vitro* (Persengiev, 2017). Although there is no direct evidence of *CEBPG* being involved in the regulation of cytokine expression in CD4 effector T cells, other C/EBP protein family members have been shown to act as negative regulators in the production of inflammatory cytokines (Berberich-Siebelt et al., 2000; Tanaka et al., 2014). Therefore, those TFs might deserve further investigation.

Selenoproteins fully rely on selenium for their biosynthesis and function. Dietary selenium supplementation in mice has been shown to increase the biosynthesis of several selenoproteins including SELS/VIMP (Stoedter et al., 2010; Tsuji et al., 2015) and to affect the expression of several inflammatory cytokines (Beck et al., 2001; Hao et al., 2016; Stoedter et al., 2010; Vunta et al., 2007; Zhu et al., 2017). Dietary selenium supplementation has further been linked to alleviate several complex and multifactorial diseases (Duffield-Lillico et al., 2003; Kim et al., 1999, 2000; Kudva et al., 2015). On the other hand, selenium deficiency might affect the synthesis of multiple selenoproteins in mice, resulting in an increased pathology from viral or bacterial infections (Beck et al., 2001; Gao et al., 2016). In our media (complete IMDM) for short-term T cell culture, the Se concentration (0.066 μM) was around 15 times lower than in human sera (~1 μM) (Rauhamaa et al., 2008; Safaralizadeh et al., 2005; Stranges et al., 2011). Although the Se concentration used in our media was low, our western blotting results (Figure 4C) have demonstrated that the Se concentration was not yet a limiting factor for VIMP protein synthesis during the tested period of up to 24 h following stimulation, as the protein expression of VIMP still increased following TCR stimulation. In the VIMP-knockdown T cells,

where the VIMP protein synthesis was further reduced, the low concentration of Se in the media was thus not a concern. Therefore, our conclusion derived from IMDM media with a VIMP-knockdown approach is reliable. Last but not least, increasing Se concentration showed a dose-dependent suppressive effect on IL2 production (Figures S1A and S1B). Following Se supplementation, the majority of the tested donors exhibited enhanced expression of VIMP in CD4 Teffs (Figure S1D). For the other donors, already having a high level of VIMP expression (Figure S1D), Se supplementation cannot further increase the expression of VIMP, but still inhibited cytokine production, possibly via enhancing the expression of the other selenoproteins as an alternative pathway. These observations indicate that at least for some patients with VIMP deficiency, Se supplementation would show beneficial values in suppressing pro-inflammatory cytokine responses of CD4 T cells.

Interestingly, the immune system presents a sexual dimorphism (Klein and Flanagan, 2016), where females appear to have a stronger humoral and cellular immune response in general, making them more resistant to infectious diseases (vom Steeg and Klein, 2016), nevertheless, more susceptible to autoimmune diseases (Angum et al., 2020; Jacobson et al., 1997). CD4 T cells, the focus of this study and the central orchestrators of immune responses, also show a differential sex-specific regulation (Afshan et al., 2012; Aldridge et al., 2018; Klein and Flanagan, 2016). Multiple factors on the genetic (Bianchi et al., 2012; Cacciari et al., 1981; Kocar et al., 2000), hormonal (Straub, 2007), or environmental level (Jensen et al., 2016; Kawai et al., 2010) have been shown to regulate sex-specific effects in immune responses. It is worth noting that selenium also displays intriguing sex-specific differences in regard to its metabolism (Seale et al., 2018), tissue distribution (Pitts et al., 2015), and effects in several physiological and pathological conditions, including immune-associated diseases (Li et al., 2020; Lu et al., 2019; Riese et al., 2006; Schomburg and Schweizer, 2009; Stoedter et al., 2010; Waters et al., 2004). Excitingly, the expression of VIMP increases following selenium supplementation in the liver of male mice, whereas in female mice VIMP expression only reaches a maximum after LPS challenge to induce an acute immune response (Stoedter et al., 2010). In regard to our data, this leads us to hypothesize that selenium supplementation and its potential sex-specific effects on VIMP expression might also result in a gender-biased effect on CD4 T cells.

Overall, using both hypothesis-free top-down computational analyses and bottom-up experimental methods, we have shown a regulatory role for the selenoprotein VIMP in controlling cytokine expression in $CD4^+CD25^-$ Teffs via several signaling pathways and transcriptional regulatory pathways. The same strategy should be generally extendable to other cell types in assisting the prediction and discovery of novel functions of any other genes of importance. In summary, our data identified an unrecognized critical regulatory role of the selenoprotein S (SELS/VIMP) in the inflammatory responses of human $CD4^+$ Teffs. Our observation provides a viable insight into how dietary supplementation of selenium might mediate its effects on $CD4^+$ Teffs and underscores the potential in therapeutically targeting VIMP in the treatment of various inflammatory and inflammation-related diseases.

Limitations of the study

Although we have successfully demonstrated an unrecognized role for *VIMP* in the regulation of CD4 T cytokine expression and the underlying mechanisms, our study still presents certain limitations. As aforementioned, selenium supplementation and immune cell responses display a sexual dimorphism. In this study, we are aware that the majority of healthy donors were male. However, due to ethic regulations, we could not specify the gender of each individual donor, making it impossible to determine a possible sex-specific effect of *VIMP* on the effector functions of CD4 T cells.

In addition, our data is based on primary human CD4 T cells expanded *in vitro* and do not take into account all the complex cellular regulatory mechanisms directly and indirectly acting on CD4 T cells present *in vivo*. Our work has shown an intrinsic role of *VIMP* on human CD4 effector T cells, but to better elucidate the importance of our findings in a disease context, *Vimp*-deficient mice could have been used, which, however, were not available in our laboratory. Even though the whole-body deficiency of some selenoproteins is embryonically lethal (Santesmasses et al., 2020), *Vimp*-deficient mice have been recently reported and mainly used to study the role of *Vimp* in muscle functions (Addinsall et al., 2018, 2020; Wright et al., 2017). Excitingly, in line with our notion in human CD4 T cells, the reduction of *Vimp* expression even in heterozygous mice has been shown to increase the expression of several inflammatory genes in fast-twitch skeletal muscles (Wright et al., 2017).

Resource availability

Lead contact

Further information and requests for different resources should be directed to and will be fulfilled by the lead contact, Feng He, Department of Infection and Immunity, Luxembourg Institute of Health, Esch-sur-Alzette, Luxembourg (feng.he@lih.lu).

Materials availability

The study did not generate any new unique materials.

Data and code availability

The whole-transcript microarray data have been deposited into Gene Expression Omnibus (GEO) repository with the access code https://www.ncbi.nlm.nih.gov/geo/query/acc.cgi?acc=GSE151266. Raw gel images from Figure 4C were deposited on Mendeley at https://doi.org/10.17632/6bd75yg6rp.1.

METHODS

All methods can be found in the accompanying Transparent methods supplemental file.

SUPPLEMENTAL INFORMATION

Supplemental information can be found online at https://doi.org/10.1016/j.isci.2021.102289.

ACKNOWLEDGMENTS

We thank Annegrät Daujeumont, Alexandre Baron, and Olga Kondratyeva for their expert technical support. We particularly appreciate Luxembourg Red Cross for providing buffy coats to us. The Feng He group was supported by Luxembourg National Research Fund (FNR) through different programs including PRIDE (CRITICS DTU)/10907093 to support C.M.C.; individual Aide à la Formation Recherche (AFR) grants PHD-2014-1/7603621 and PHD-2015-1/9989160 to support E.D. and N.Z. respectively; and intramural funding within Luxembourg Institute of Health and Luxembourg Center for Systems Biomedicine from Ministère de l'Enseignement supérieur et de la Recherche (MESR). M.O. was supported as coordinator by FNR through the FNR PRIDE program for a doctoral training unit (DTU, PRIDE/NEXTIMMUNE/11012546). Some icons in the graphical abstract were created with BioRender.com.

AUTHOR CONTRIBUTIONS

C.M.C., N.Z., E.D. designed and performed experiments. C.M.C. analyzed the data and wrote the manuscript. S.F.R. performed parts of the experiments. R.B., M.O., and F.Q.H. supervised the project. F.Q.H. designed the project, oversaw the whole project, and revised the manuscript. All the authors read and edited the manuscript.

DECLARATION OF INTERESTS

The authors declare that they have no conflict of interest.

INCLUSION AND DIVERSITY

We worked to ensure ethnic or other types of diversity in the recruitment of human subjects. The author list of this paper includes contributors from the location where the research was conducted who participated in the data collection, design, analysis, and/or interpretation of the work.

Received: July 24, 2020
Revised: February 8, 2021
Accepted: March 5, 2021
Published: April 23, 2021

REFERENCES

Addinsall, A.B., Wright, C.R., Kotsiakos, T.L., Smith, Z.M., Cook, T.R., Andrikopoulos, S., van der Poel, C., and Stupka, N. (2020). Impaired exercise performance is independent of inflammation and cellular stress following genetic reduction or deletion of selenoprotein S. Am. J. Physiol. Regul. Integr. Comp. Physiol. *318*, R981–R996.

Addinsall, A.B., Wright, C.R., Shaw, C.S., McRae, N.L., Forgan, L.G., Weng, C.H., Conlan, X.A., Francis, P.S., Smith, Z.M., Andrikopoulos, S., et al. (2018). Deficiency of selenoprotein S, an endoplasmic reticulum resident oxidoreductase, impairs the contractile function of fast-twitch hindlimb muscles. Am. J. Physiol. Regul. Integr. Comp. Physiol. *315*, R380–R396.

Afshan, G., Afzal, N., and Qureshi, S. (2012). CD4+CD25(hi) regulatory T cells in healthy males and females mediate gender difference in the prevalence of autoimmune diseases. Clin. Lab. *58*, 567–571.

Alanne, M., Kristiansson, K., Auro, K., Silander, K., Kuulasmaa, K., Peltonen, L., Salomaa, V., and Perola, M. (2007). Variation in the selenoprotein S gene locus is associated with coronary heart disease and ischemic stroke in two independent Finnish cohorts. Hum. Genet. *122*, 355–365.

Aldridge, J., Pandya, J.M., Meurs, L., Andersson, K., Nordström, I., Theander, E., Lundell, A.C., and Rudin, A. (2018). Sex-based differences in association between circulating T cell subsets and disease activity in untreated early rheumatoid arthritis patients. Arthritis Res. Ther. *20*, 150.

Angum, F., Khan, T., Kaler, J., Siddiqui, L., and Hussain, A. (2020). The prevalence of autoimmune disorders in women: a narrative review. Cureus *12*, e8094.

Beck, M.A., Nelson, H.K., Shi, Q., Van Dael, P., Schiffrin, E.J., Blum, S., Barclay, D., and Levander, O.A. (2001). Selenium deficiency increases the pathology of an influenza virus infection. FASEB J. *15*, 1481–1483.

Berberich-Siebelt, F., Klein-Hessling, S., Hepping, N., Santner-Nanan, B., Lindemann, D., Schimpl, A., Berberich, I., and Serfling, E. (2000). C/EBPβ enhances IL-4 but impairs IL-2 and IFN-γ induction in T cells. Eur. J. Immunol. *30*, 2576–2585.

Beyer, A., Bandyopadhyay, S., and Ideker, T. (2007). Integrating physical and genetic maps: from genomes to interaction networks. Nat. Rev. Genet. *8*, 699–710.

Bianchi, I., Lleo, A., Gershwin, M.E., and Invernizzi, P. (2012). The X chromosome and immune associated genes. J. Autoimmun. *38*, J187–J192.

Braun, J., Loyal, L., Frentsch, M., Wendisch, D., Georg, P., Kurth, F., Hippenstiel, S., Dingeldey, M., Kruse, B., Fauchere, F., et al. (2020). SARS-CoV-2-reactive T cells in healthy donors and patients with COVID-19. Nature *587*, 270–274.

Brennan, P., Babbage, J.W., Burgering, B.M., Groner, B., Reif, K., and Cantrell, D.A. (1997). Phosphatidylinositol 3-kinase couples the interleukin-2 receptor to the cell cycle regulator E2F. Immunity *7*, 679–689.

Brownlie, R.J., and Zamoyska, R. (2013). T cell receptor signalling networks: branched, diversified and bounded. Nat. Rev. Immunol. *13*, 257–269.

Cacciari, E., Masi, M., Fantini, M.P., Licastro, F., Cicognani, A., Pirazzoli, P., Villa, M.P., Specchia, F., Forabosco, A., Franceschi, C., et al. (1981). Serum immunoglobulins and lymphocyte subpopulations derangement in Turner's syndrome. J. Immunogenet. *8*, 337–344.

Chow, C.W., Rincon, M., and Davis, R.J. (1999). Requirement for transcription factor NFAT in interleukin-2 expression. Mol. Cell Biol. *19*, 2300–2307.

Curran, J.E., Jowett, J.B., Elliott, K.S., Gao, Y., Gluschenko, K., Wang, J., Abel Azim, D.M., Cai, G., Mahaney, M.C., Comuzzie, A.G., et al. (2005). Genetic variation in selenoprotein S influences inflammatory response. Nat. Genet. *37*, 1234–1241.

Danileviciute, E., Zeng, N., Capelle, C., Paczia, N., Gillespie, M.A., Kurniawan, H., Coowar, D., Vogt Weisenhorn, D.M., Giro, G.G., Grusdat, M., et al. (2019). PARK7/DJ-1 promotes pyruvate dehydrogenase activity and maintains Treg homeostasis. https://doi.org/10.1101/2019.12.20.884809.

Duffield-Lillico, A.J., Dalkin, B.L., Reid, M.E., Turnbull, B.W., Slate, E.H., Jacobs, E.T., Marshall, J.R., Clark, L.C., and Nutritional Prevention of Cancer Study, G. (2003). Selenium supplementation, baseline plasma selenium status and incidence of prostate cancer: an analysis of the complete treatment period of the Nutritional Prevention of Cancer Trial. BJU Int. *91*, 608–612.

Fradejas, N., Serrano-Perez Mdel, C., Tranque, P., and Calvo, S. (2011). Selenoprotein S expression in reactive astrocytes following brain injury. Glia *59*, 959–972.

Gao, X., Zhang, Z., Li, Y., Shen, P., Hu, X., Cao, Y., and Zhang, N. (2016). Selenium deficiency facilitates inflammation following S. aureus infection by regulating TLR2-related pathways in the mouse mammary gland. Biol. Trace Elem. Res. *172*, 449–457.

Gillis, J., and Pavlidis, P. (2011). The role of indirect connections in gene networks in predicting function. Bioinformatics *27*, 1860–1866.

Hao, S., Hu, J., Song, S., Huang, D., Xu, H., Qian, G., Gan, F., and Huang, K. (2016). Selenium alleviates aflatoxin B(1)-induced immune toxicity through improving glutathione peroxidase 1 and selenoprotein S expression in primary porcine splenocytes. J. Agric. Food Chem. *64*, 1385–1393.

He, F., Chen, H., Probst-Kepper, M., Geffers, R., Eifes, S., Del Sol, A., Schughart, K., Zeng, A.P., and Balling, R. (2012). PLAU inferred from a correlation network is critical for suppressor function of regulatory T cells. Mol. Syst. Biol. *8*, 624.

He, F.Q., and Ollert, M. (2016). Network-guided key gene discovery for a given cellular process. Adv. Biochem. Eng. Biotechnol.

He, L., Wang, B., Yao, Y., Su, M., Ma, H., and Jia, N. (2014). Protective effects of the SEPS1 gene on lipopolysaccharide-induced sepsis. Mol. Med. Rep. *9*, 1869–1876.

Hogan, P.G., Chen, L., Nardone, J., and Rao, A. (2003). Transcriptional regulation by calcium, calcineurin, and NFAT. Genes Dev. *17*, 2205–2232.

Ingham, A.B., Osborne, S.A., Menzies, M., Briscoe, S., Chen, W., Kongsuwan, K., Reverter, A., Jeanes, A., Dalrymple, B.P., Wijffels, G., et al. (2014). RNF14 is a regulator of mitochondrial and immune function in muscle. BMC Syst. Biol. *8*, 10.

Jacobson, D.L., Gange, S.J., Rose, N.R., and Graham, N.M. (1997). Epidemiology and estimated population burden of selected autoimmune diseases in the United States. Clin. Immunol. Immunopathol *84*, 223–243.

Jensen, K.J., Fisker, A.B., Andersen, A., Sartono, E., Yazdanbakhsh, M., Aaby, P., Erikstrup, C., and Benn, C.S. (2016). The effects of vitamin A supplementation with measles vaccine on leucocyte counts and in vitro cytokine production. Br. J. Nutr. *115*, 619–628.

Joost, S., Zeisel, A., Jacob, T., Sun, X., La Manno, G., Lönnerberg, P., Linnarsson, S., and Kasper, M. (2016). Single-cell transcriptomics reveals that differentiation and spatial signatures shape epidermal and hair follicle heterogeneity. Cell Syst. *3*, 221–237.e9.

Karlsson, H.K., Lake, S., Koistinen, H.A., and Krook, A. (2004). Relationship between serum amyloid A level and Tanis/SelS mRNA expression in skeletal muscle and adipose tissue from healthy and type 2 diabetic subjects. Diabetes *53*, 1424–1428.

Kawai, K., Msamanga, G., Manji, K., Villamor, E., Bosch, R.J., Hertzmark, E., and Fawzi, W.W. (2010). Sex differences in the effects of maternal vitamin supplements on mortality and morbidity among children born to HIV-infected women in Tanzania. Br. J. Nutr. *103*, 1784–1791.

Kim, H.-C., Jhoo, W.-K., Choi, D.-Y., Im, D.-H., Shin, E.-J., Suh, J.-H., Floyd, R.A., and Bing, G. (1999). Protection of methamphetamine nigrostriatal toxicity by dietary selenium. Brain Res. *851*, 76–86.

Kim, H.-C., Jhoo, W.-K., Shin, E.-J., and Bing, G. (2000). Selenium deficiency potentiates methamphetamine-induced nigral neuronal loss; comparison with MPTP model. Brain Res. *862*, 247–252.

Kim, K.H., Gao, Y., Walder, K., Collier, G.R., Skelton, J., and Kissebah, A.H. (2007). SEPS1 protects RAW264.7 cells from pharmacological ER stress agent-induced apoptosis. Biochem. Biophys. Res. Commun. *354*, 127–132.

Klein, S.L., and Flanagan, K.L. (2016). Sex differences in immune responses. Nat. Rev. Immunol. *16*, 626–638.

Kocar, I.H., Yesilova, Z., Ozata, M., Turan, M., Sengul, A., and Ozdemir, I. (2000). The effect of testosterone replacement treatment on immunological features of patients with

Klinefelter's syndrome. Clin. Exp. Immunol. *121*, 448–452.

Kuchroo, V.K., Ohashi, P.S., Sartor, R.B., and Vinuesa, C.G. (2012). Dysregulation of immune homeostasis in autoimmune diseases. Nat. Med. *18*, 42–47.

Kudva, A.K., Shay, A.E., and Prabhu, K.S. (2015). Selenium and inflammatory bowel disease. Am. J. Physiol. Gastrointest. Liver Physiol. *309*, G71–G77.

Langfelder, P., and Horvath, S. (2008). WGCNA: an R package for weighted correlation network analysis. BMC Bioinformatics *9*, 559.

Lee, A.H., Iwakoshi, N.N., and Glimcher, L.H. (2003). XBP-1 regulates a subset of endoplasmic reticulum resident chaperone genes in the unfolded protein response. Mol. Cell Biol *23*, 7448–7459.

Lee, J.H., Park, K.J., Jang, J.K., Jeon, Y.H., Ko, K.Y., Kwon, J.H., Lee, S.R., and Kim, I.Y. (2015). Selenoprotein S-dependent selenoprotein K binding to p97(VCP) protein is essential for endoplasmic reticulum-associated degradation. J. Biol. Chem. *290*, 29941–29952.

Li, J., Lo, K., Shen, G., Feng, Y.Q., and Huang, Y.Q. (2020). Gender difference in the association of serum selenium with all-cause and cardiovascular mortality. Postgrad. Med. *132*, 148–155.

Liu, X., Zhang, P., Bao, Y., Han, Y., Wang, Y., Zhang, Q., Zhan, Z., Meng, J., Li, Y., Li, N., et al. (2013). Zinc finger protein ZBTB20 promotes Toll-like receptor-triggered innate immune responses by repressing IkappaBalpha gene transcription. Proc. Natl. Acad. Sci. U S A *110*, 11097–11102.

Lu, C.W., Chang, H.H., Yang, K.C., Chiang, C.H., Yao, C.A., and Huang, K.C. (2019). Gender differences with Dose(-)Response relationship between serum selenium levels and metabolic syndrome-A case-control study. Nutrients *11*, 477.

Martinez, A., Santiago, J.L., Varade, J., Marquez, A., Lamas, J.R., Mendoza, J.L., de la Calle, H., Diaz-Rubio, M., de la Concha, E.G., Fernandez-Gutierrez, B., et al. (2008). Polymorphisms in the selenoprotein S gene: lack of association with autoimmune inflammatory diseases. BMC Genomics *9*, 329.

Mathew, D., Giles, J.R., Baxter, A.E., Oldridge, D.A., Greenplate, A.R., Wu, J.E., Alanio, C., Kuri-Cervantes, L., Pampena, M.B., D'Andrea, K., et al. (2020). Deep immune profiling of COVID-19 patients reveals distinct immunotypes with therapeutic implications. Science *369*, eabc8511.

McGuckin, M.A., Eri, R.D., Das, I., Lourie, R., and Florin, T.H. (2010). ER stress and the unfolded protein response in intestinal inflammation. Am. J. Physiol. Gastrointest. Liver Physiol. *298*, G820–G832.

Meplan, C., Hughes, D.J., Pardini, B., Naccarati, A., Soucek, P., Vodickova, L., Hlavata, I., Vrana, D., Vodicka, P., and Hesketh, J.E. (2010). Genetic variants in selenoprotein genes increase risk of colorectal cancer. Carcinogenesis *31*, 1074–1079.

Okamura, H., Aramburu, J., Garcia-Rodriguez, C., Viola, J.P., Raghavan, A., Tahiliani, M., Zhang, X., Qin, J., Hogan, P.G., and Rao, A. (2000). Concerted dephosphorylation of the transcription factor NFAT1 induces a conformational switch that regulates transcriptional activity. Mol. Cell *6*, 539–550.

Oliver, S. (2000). Guilt-by-association goes global. Nature *403*, 601–603.

Olsson, M., Olsson, B., Jacobson, P., Thelle, D.S., Bjorkegren, J., Walley, A., Froguel, P., Carlsson, L.M., and Sjoholm, K. (2011). Expression of the selenoprotein S (SELS) gene in subcutaneous adipose tissue and SELS genotype are associated with metabolic risk factors. Metabolism *60*, 114–120.

Persengiev, S.P. (2017). Identification of an essential IL15-STAT1-IRX3 prosurvival pathway in T lymphocytes with therapeutic implications. bioRxiv, 178939.

Pitts, M.W., and Hoffmann, P.R. (2018). Endoplasmic reticulum-resident selenoproteins as regulators of calcium signaling and homeostasis. Cell Calcium *70*, 76–86.

Pitts, M.W., Kremer, P.M., Hashimoto, A.C., Torres, D.J., Byrns, C.N., Williams, C.S., and Berry, M.J. (2015). Competition between the brain and testes under selenium-compromised conditions: insight into sex differences in selenium metabolism and risk of neurodevelopmental disease. J. Neurosci. *35*, 15326–15338.

Qin, H.S., Yu, P.P., Sun, Y., Wang, D.F., Deng, X.F., Bao, Y.L., Song, J., Sun, L.G., Song, Z.B., and Li, Y.X. (2016). Paclitaxel inhibits selenoprotein S expression and attenuates endoplasmic reticulum stress. Mol. Med. Rep. *13*, 5118–5124.

Rauhamaa, P., Kantola, M., Viitak, A., Kaasik, T., and Mussalo-Rauhamaa, H. (2008). Selenium levels of Estonians. Eur. J. Clin. Nutr. *62*, 1075–1078.

Riese, C., Michaelis, M., Mentrup, B., Götz, F., Köhrle, J., Schweizer, U., and Schomburg, L. (2006). Selenium-dependent pre- and posttranscriptional mechanisms are responsible for sexual dimorphic expression of selenoproteins in murine tissues. Endocrinology *147*, 5883–5892.

Rodriguez-Jorge, O., Kempis-Calanis, L.A., Abou-Jaoude, W., Gutierrez-Reyna, D.Y., Hernandez, C., Ramirez-Pliego, O., Thomas-Chollier, M., Spicuglia, S., Santana, M.A., and Thieffry, D. (2019). Cooperation between T cell receptor and Toll-like receptor 5 signaling for CD4(+) T cell activation. Sci. Signal. *12*, eaar3641.

Saez-Rodriguez, J., Simeoni, L., Lindquist, J.A., Hemenway, R., Bommhardt, U., Arndt, B., Haus, U.U., Weismantel, R., Gilles, E.D., Klamt, S., et al. (2007). A logical model provides insights into T cell receptor signaling. PLoS Comput. Biol. *3*, e163.

Safaralizadeh, R., Kardar, G.A., Pourpak, Z., Moin, M., Zare, A., and Teimourian, S. (2005). Serum concentration of selenium in healthy individuals living in Tehran. Nutr. J. *4*, 32.

Santesmasses, D., Mariotti, M., and Gladyshev, V.N. (2020). Tolerance to selenoprotein loss differs between human and mouse. Mol. Biol. Evol. *37*, 341–354.

Santos, L.R., Duraes, C., Mendes, A., Prazeres, H., Alvelos, M.I., Moreira, C.S., Canedo, P., Esteves, C., Neves, C., Carvalho, D., et al. (2014). A polymorphism in the promoter region of the selenoprotein S gene (SEPS1) contributes to Hashimoto's thyroiditis susceptibility. J. Clin. Endocrinol. Metab. *99*, E719–E723.

Schomburg, L. (2011). Selenium, selenoproteins and the thyroid gland: interactions in health and disease. Nat. Rev. Endocrinol. *8*, 160–171.

Schomburg, L., and Schweizer, U. (2009). Hierarchical regulation of selenoprotein expression and sex-specific effects of selenium. Biochim. Biophys. Acta *1790*, 1453–1462.

Seale, L.A., Ogawa-Wong, A.N., and Berry, M.J. (2018). Sexual dimorphism in selenium metabolism and selenoproteins. Free Radic. Biol. Med. *127*, 198–205.

Seiderer, J., Dambacher, J., Kuhnlein, B., Pfennig, S., Konrad, A., Torok, H.P., Haller, D., Goke, B., Ochsenkuhn, T., Lohse, P., et al. (2007). The role of the selenoprotein S (SELS) gene -105G>A promoter polymorphism in inflammatory bowel disease and regulation of SELS gene expression in intestinal inflammation. Tissue Antigens *70*, 238–246.

Sharma, S., Findlay, G.M., Bandukwala, H.S., Oberdoerffer, S., Baust, B., Li, Z., Schmidt, V., Hogan, P.G., Sacks, D.B., and Rao, A. (2011). Dephosphorylation of the nuclear factor of activated T cells (NFAT) transcription factor is regulated by an RNA-protein scaffold complex. Proc. Natl. Acad. Sci. U S A *108*, 11381–11386.

Shibata, T., Arisawa, T., Tahara, T., Ohkubo, M., Yoshioka, D., Maruyama, N., Fujita, H., Kamiya, Y., Nakamura, M., Nagasaka, M., et al. (2009). Selenoprotein S (SEPS1) gene -105G>A promoter polymorphism influences the susceptibility to gastric cancer in the Japanese population. BMC Gastroenterol. *9*, 2.

Speckmann, B., Gerloff, K., Simms, L., Oancea, I., Shi, W., McGuckin, M.A., Radford-Smith, G., and Khanna, K.K. (2014). Selenoprotein S is a marker but not a regulator of endoplasmic reticulum stress in intestinal epithelial cells. Free Radic. Biol. Med. *67*, 265–277.

Stoedter, M., Renko, K., Hog, A., and Schomburg, L. (2010). Selenium controls the sex-specific immune response and selenoprotein expression during the acute-phase response in mice. Biochem. J. *429*, 43–51.

Stranges, S., Tabák, A.G., Guallar, E., Rayman, M.P., Akbaraly, T.N., Laclaustra, M., Alfthan, G., Mussalo-Rauhamaa, H., Viikari, J.S., Raitakari, O.T., et al. (2011). Selenium status and blood lipids: the cardiovascular risk in Young Finns study. J. Intern. Med. *270*, 469–477.

Straub, R.H. (2007). The complex role of estrogens in inflammation. Endocr. Rev. *28*, 521–574.

Sutherland, A., Kim, D.H., Relton, C., Ahn, Y.O., and Hesketh, J. (2010). Polymorphisms in the selenoprotein S and 15-kDa selenoprotein genes are associated with altered susceptibility to colorectal cancer. Genes Nutr. *5*, 215–223.

Szklarczyk, D., Gable, A.L., Lyon, D., Junge, A., Wyder, S., Huerta-Cepas, J., Simonovic, M.,

Doncheva, N.T., Morris, J.H., Bork, P., et al. (2019). STRING v11: protein-protein association networks with increased coverage, supporting functional discovery in genome-wide experimental datasets. Nucleic Acids Res. *47*, D607–D613.

Tanaka, S., Tanaka, K., Magnusson, F., Chung, Y., Martinez, G.J., Wang, Y.H., Nurieva, R.I., Kurosaki, T., and Dong, C. (2014). CCAAT/enhancer-binding protein alpha negatively regulates IFN-gamma expression in T cells. J. Immunol. *193*, 6152–6160.

Tsuji, P.A., Carlson, B.A., Anderson, C.B., Seifried, H.E., Hatfield, D.L., and Howard, M.T. (2015). Dietary selenium levels affect selenoprotein expression and support the interferon-gamma and IL-6 immune response pathways in mice. Nutrients *7*, 6529–6549.

van Dam, S., Vosa, U., van der Graaf, A., Franke, L., and de Magalhaes, J.P. (2018). Gene co-expression analysis for functional classification and gene-disease predictions. Brief Bioinform. *19*, 575–592.

vom Steeg, L.G., and Klein, S.L. (2016). SeXX matters in infectious disease pathogenesis. PLoS Pathog. *12*, e1005374.

Vunta, H., Davis, F., Palempalli, U.D., Bhat, D., Arner, R.J., Thompson, J.T., Peterson, D.G., Reddy, C.C., and Prabhu, K.S. (2007). The anti-inflammatory effects of selenium are mediated through 15-deoxy-Delta12,14-prostaglandin J2 in macrophages. J. Biol. Chem. *282*, 17964–17973.

Waters, D.J., Chiang, E.C., Cooley, D.M., and Morris, J.S. (2004). Making sense of sex and supplements: differences in the anticarcinogenic effects of selenium in men and women. Mutat. Res. *551*, 91–107.

Wright, C.R., Allsopp, G.L., Addinsall, A.B., McRae, N.L., Andrikopoulos, S., and Stupka, N. (2017). A reduction in selenoprotein S amplifies the inflammatory profile of fast-twitch skeletal muscle in the mdx dystrophic mouse. Mediators Inflamm. *2017*, 7043429.

Ye, Y., Shibata, Y., Kikkert, M., van Voorden, S., Wiertz, E., and Rapoport, T.A. (2005). Recruitment of the p97 ATPase and ubiquitin ligases to the site of retrotranslocation at the endoplasmic reticulum membrane. Proc. Natl. Acad. Sci. U S A *102*, 14132–14138.

Ye, Y., Shibata, Y., Yun, C., Ron, D., and Rapoport, T.A. (2004). A membrane protein complex mediates retro-translocation from the ER lumen into the cytosol. Nature *429*, 841–847.

Yoshida, H., Matsui, T., Yamamoto, A., Okada, T., and Mori, K. (2001). XBP1 mRNA is induced by ATF6 and spliced by IRE1 in response to ER stress to produce a highly active transcription factor. Cell *107*, 881–891.

Zhang, H.M., Chen, H., Liu, W., Liu, H., Gong, J., Wang, H., and Guo, A.Y. (2012). AnimalTFDB: a comprehensive animal transcription factor database. Nucleic Acids Res. *40*, D144–D149.

Zhang, W., Mi, J., Li, N., Sui, L., Wan, T., Zhang, J., Chen, T., and Cao, X. (2001). Identification and characterization of DPZF, a novel human BTB/POZ zinc finger protein sharing homology to BCL-6. Biochem. Biophys. Res. Commun. *282*, 1067–1073.

Zhu, C., Chen, G., Zhao, Y., Gao, X.M., and Wang, J. (2018). Regulation of the development and function of B cells by ZBTB transcription factors. Front. Immunol. *9*, 580.

Zhu, C., Zhang, S., Song, C., Zhang, Y., Ling, Q., Hoffmann, P.R., Li, J., Chen, T., Zheng, W., and Huang, Z. (2017). Selenium nanoparticles decorated with Ulva lactuca polysaccharide potentially attenuate colitis by inhibiting NF-kappaB mediated hyper inflammation. J. Nanobiotechnol. *15*, 20.

Zhu, J., and Paul, W.E. (2010a). Heterogeneity and plasticity of T helper cells. Cell Res. *20*, 4–12.

Zhu, J., and Paul, W.E. (2010b). Peripheral CD4+ T-cell differentiation regulated by networks of cytokines and transcription factors. Immunol. Rev. *238*, 247–262.

iScience, Volume *24*

Supplemental information

Identification of VIMP as a gene inhibiting cytokine production in human CD4+ effector T cells

Christophe M. Capelle, Ni Zeng, Egle Danileviciute, Sabrina Freitas Rodrigues, Markus Ollert, Rudi Balling, and Feng Q. He

Supplemental Information

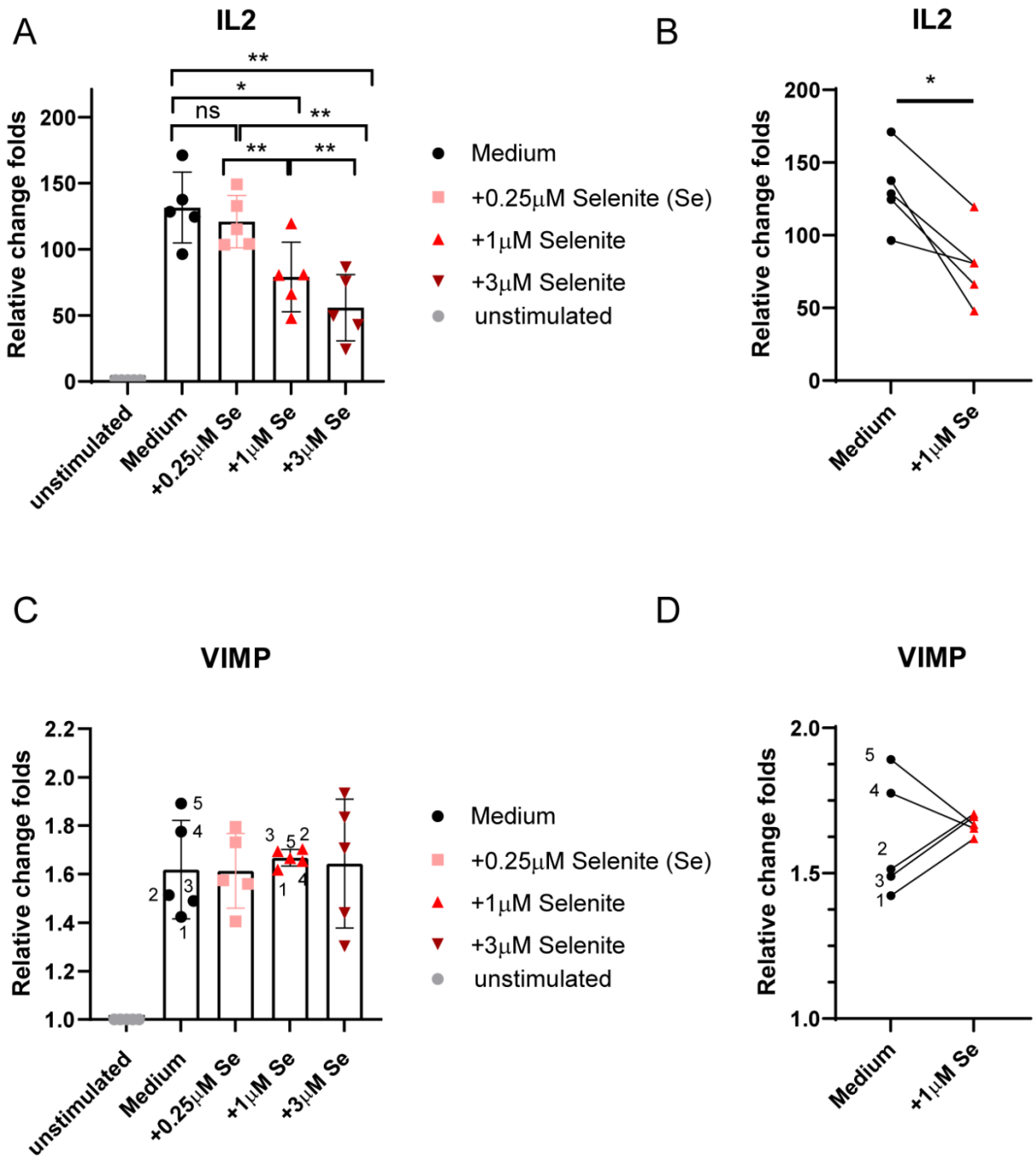

Supplemental Figure S1. Selenium supplementation suppresses IL2 production in CD4 Teffs, Related to Figure 2. Human CD4+CD25- T cells sorted from healthy donors were unstimulated in normal IMDM complete media or stimulated for 24 hrs by soluble anti-CD3/CD28 antibodies either in IMDM complete media alone or supplemented with different concentration of sodium selenite (S5261, Sigma Aldrich). (**A, C**) The mRNA expression of IL2 (**A**) and VIMP (**C**) was quantified by qPCR and normalized to the housekeeping gene RPS9 and to that of the unstimulated samples of the given donor. (**B, D)** A "zooming-in" analysis of the two selected concentrations of Se for IL2 (**B**) and VIMP (**D**). Each dot represents one heathy donor. The donor ID was indicated for the concentration of interests. Data are mean± standard deviation (s.d.). The P-values are determined

by a two-tailed paired Student’s t test. ns or unlabeled, non-significant; *P<=0.05, **P<=0.01 and ***P<=0.001.

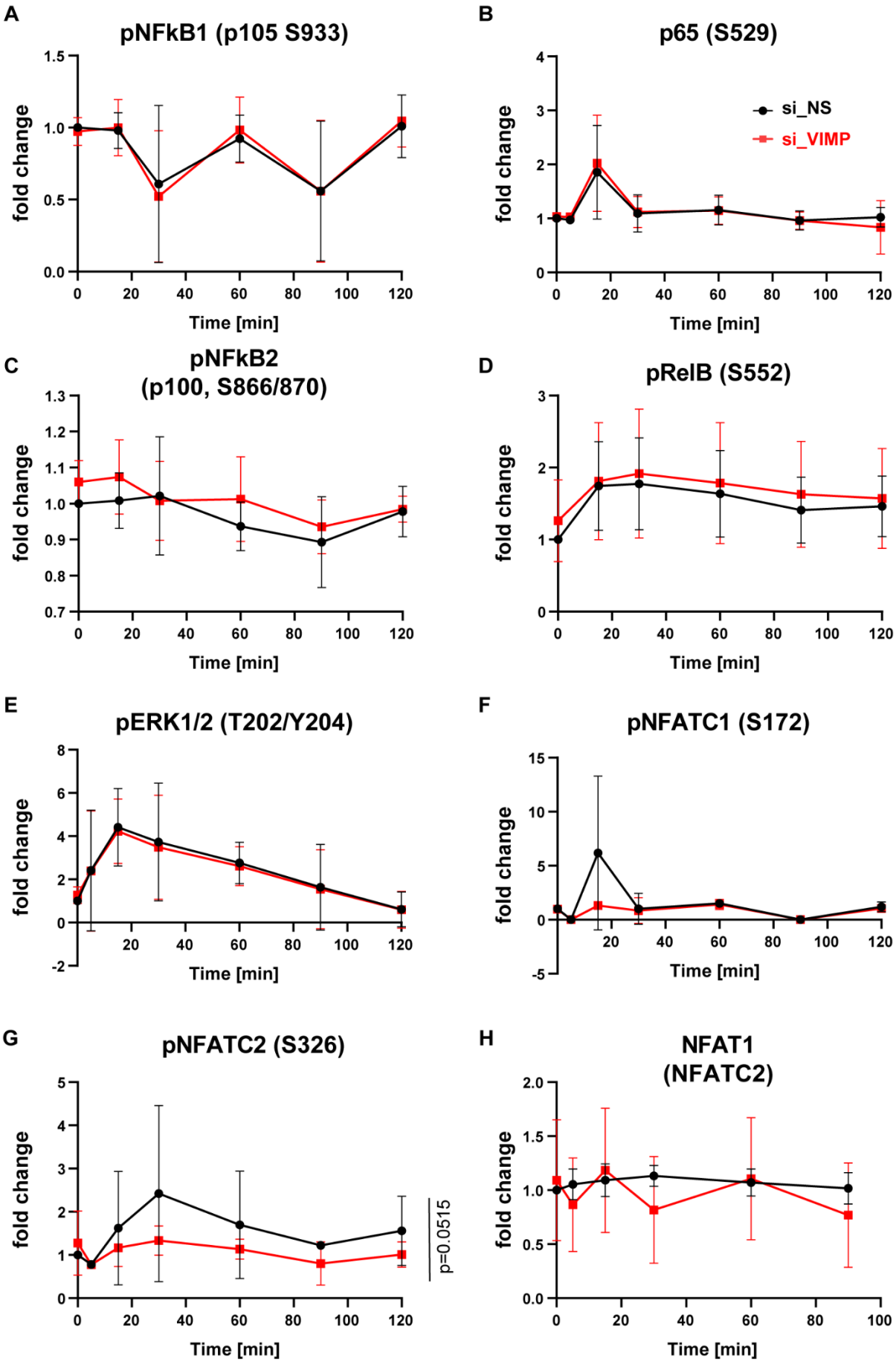
A
pNFkB1 (p105 S933)
fold change
Time [min]
B
p65 (S529)
si_NS
si_VIMP
fold change
Time [min]
C
pNFkB2
(p100, S866/870)
fold change
Time [min]
D
pRelB (S552)
fold change
Time [min]
E
pERK1/2 (T202/Y204)
fold change
Time [min]
F
pNFATC1 (S172)
fold change
Time [min]
G
pNFATC2 (S326)
fold change
Time [min]
p=0.0515
H
NFAT1
(NFATC2)
fold change
Time [min]

Supplemental Figure S2. VIMP knockdown only affects the phosphorylation of NFATC2, not the other major signaling pathways downstream of the TCR, Related to Figure 4.

Phosphorylation of proteins involved in the major signaling pathways downstream of TCR signaling in Teffs, assessed by flow cytometry at different time points following PMA/Ionomycin stimulation. Before stimulation, the cells were transfected with specific siRNA against VIMP (si_VIMP) versus non-specific siRNA (si_NS) for 1 day. (**G**) Only pNFATC2 was significantly decreased by VIMP knockdown. The other measured targets remain no significant change (**A**-**F, H**). The fold change was calculated by normalizing the geometric mean (Geomean) of the fluorescence intensities of all the conditions to that of the unstimulated control knockdown condition. Data are mean± standard deviation (s.d.). The P-values are determined by a two-tailed paired Student's t test over time including the data at different time points. ns or unlabeled, non-significant; *P<=0.05, **P<=0.01 and ***P<=0.001. All the graphs represent the pooled flow cytometry data for the fold change from 2-7 independent donors.

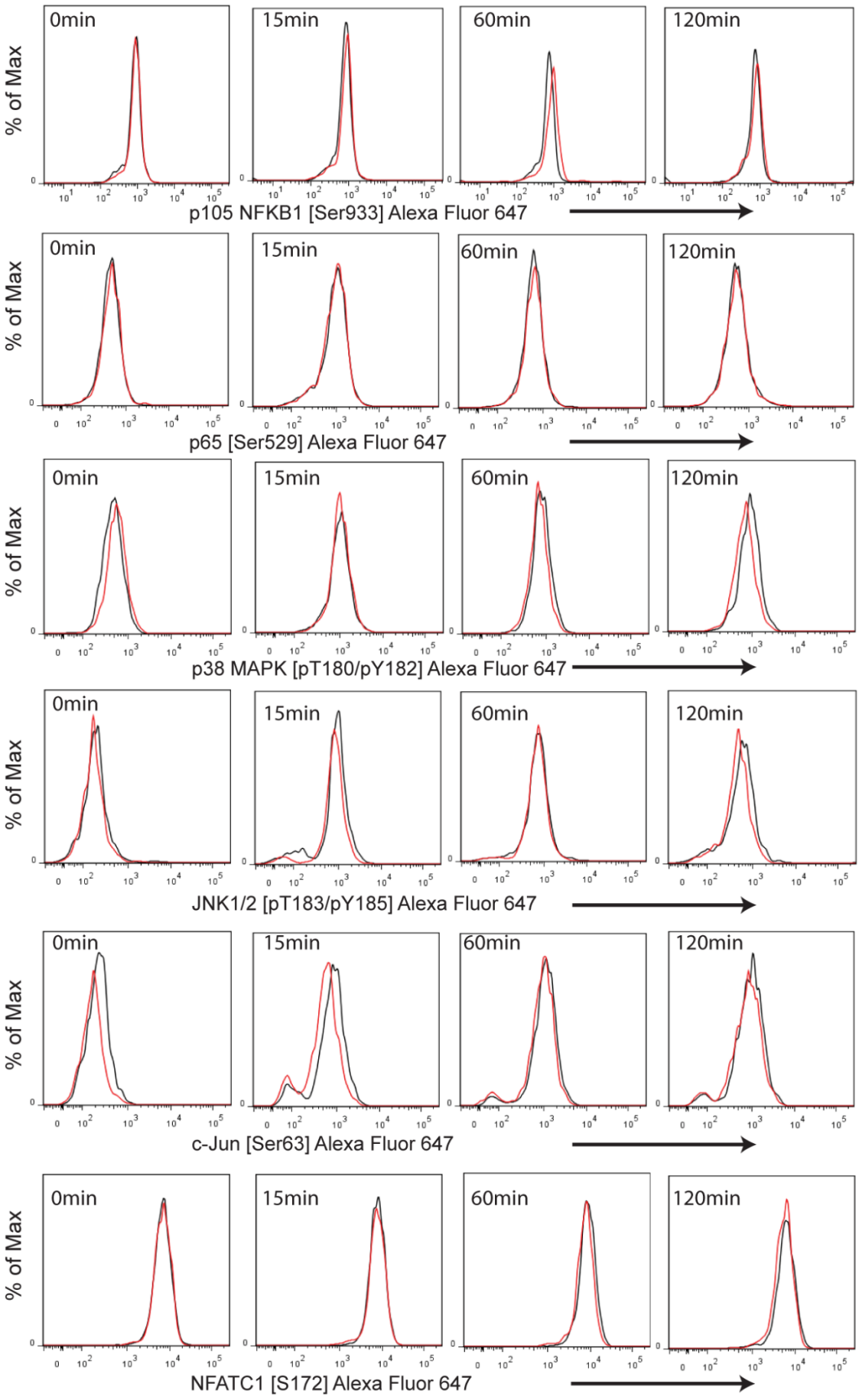
0min
15min
60min
120min
% of Max
p105 NFKB1 [Ser933] Alexa Fluor 647
p65 [Ser529] Alexa Fluor 647
p38 MAPK [pT180/pY182] Alexa Fluor 647
JNK1/2 [pT183/pY185] Alexa Fluor 647
c-Jun [Ser63] Alexa Fluor 647
NFATC1 [S172] Alexa Fluor 647

Supplemental Figure S3. VIMP knockdown does not affect other major signaling pathways downstream of the TCR, Related to Figure 4.

Representative histogram overlay for the phosphorylation of major signaling transduction proteins downstream of the TCR signaling in Teffs, assessed by flow cytometry at different time points following PMA/Ionomycin stimulation. Before stimulation, the cells were first transfected with specific siRNA against VIMP (si_VIMP) versus non-specific siRNA (si_NS) for 1 day. No significant effects on the phosphorylation levels of MAPK (p38, ERK1/2, cJun, JNK1/2) pathways and canonical (p65, p105) or non-canonical (RELB, NFκB2) NFκB pathways during the first 120 min stimulation after siRNA knockdown in Teffs. The expression of total NFAT1 protein was also unaffected by VIMP knockdown. The numbers in x-axis indicate the geometric mean (Geomean) fluorescence intensity of the different proteins or phosphorylation sites. Data are mean± standard deviation (s.d.). The other measured targets remain no significant change (**A**-**G**). The P-values are determined by a two-tailed paired Student's t test. ns or unlabeled, non-significant; *P<=0.05, **P<=0.01 and ***P<=0.001. All the graphs represent data from 2-7 independent donors.

Transparent Methods

Primary T cell isolation and culture

Buffy coats from healthy donors were provided by the Red Cross Luxembourg and the informed consent was obtained from each donor by the Red Cross Luxembourg. The T cell isolation and culture procedures have been described in our previous works (Danileviciute et al., 2019; He et al., 2012; Sawlekar et al., 2020). For the requirement of the STAR methods, we briefly described it here again. We added the RosetteSep™ Human CD4+ T cell Enrichment Cocktail (15062, Stemcell) to undiluted blood at a concentration of 50 µl/ml and incubated for 30 min at 4°C. The incubated samples were then diluted 2 times with FACS buffer (PBS + 2% FBS) and the CD4+ T cells were obtained following gradient centrifugation at 1200 g for 20 min, using Lympoprep (07801, StemCell) and SepMate™-50 tubes (85450, Stemcell). Before sorting, the CD4+ T cells were first stained with mouse monoclonal [RPA-T4] anti-human CD4 FITC (555346, BD Biosciences) (dilution 1:20), mouse monoclonal [M-A251] anti-human CD25 APC (555434, BD Biosciences) (dilution 1:20) and LIVE/DEAD® Fixable Near-IR Dead Cell Stain (L10119, Thermo Fisher Scientific) (dilution 1:500). Primary CD4 T cells ($CD4^+CD25^-$) were then sorted on a BD FACSAria™ III cell sorter (BD Biosciences).

Target	Fluorochromes	Dilution	Company	Clone	Reference
CD4	FITC	1:20	BD Biosciences	RPA-T4	555346
CD25	APC	1:20	BD Biosciences	M-A251	555434
Live/Dead	Near Infra-Red	1:500	Thermo Fisher Scientific	N.A.	L10119

Sorted human CD4+ T cells were cultured in IMDM (21980-032, Thermo Fisher Scientific) complete medium, supplemented with 10% heat-inactivated (56°C, 45 min) fetal bovine serum (FBS) (10500-064, Thermo Fisher Scientific), 1x Penicillin+Streptomycin (15070-063, Thermo Fisher Scientific), 1x MEM non-essential amino acids (M7145, Sigma-Aldrich) and 1x β-mercaptoethanol (21985-023,

Thermo Fisher Scientific). Every seven days for a maximum of four weeks, Teffs were derived from isolated $CD4^+CD25^-$ T cells by restimulating them with irradiated Epstein–Barr virus (EBV) transformed B-cells (EBV-B cells) (Probst-Kepper et al., 2009), at a 1:1 ratio to expand and maintain the culture. The EBV-B cells were irradiated in RS2000 X-Ray Biological Irradiator (Rad Source Technologies) for 30 min with a total of 90 Gy.

Teff siRNA knockdown and stimulation

Targeted gene's expression was knocked-down in up to 5 x 10^6 cells using the P3 Primary Cell 4D-Nucleofector X Kit L (V4XP-3024, Lonza) with 90 µl P3 Primary cell solution and 100 pmol of corresponding si_RNA (resuspended in 10 ul RNAse-free H2O): si_Non-Specific scrambled control siRNA (si_NS or si_CTRL) (SC-37007, Santa Cruz), si_VIMP/SELS (SI03053512, Qiagen), si_E2F5 (SI00030436, Qiagen). siRNA transfection by electroporation was performed in the Amaxa 4D-Nucleofector™ X System (Lonza) according to the manufacturer's recommended program for primary human T cells (with the program code EO-115). Following transfection, the Teffs were first transferred into a 12-well plate with pre-warmed complete IMDM medium and incubated at 37 °C for 24 hrs before being stimulated with 25 µl/ml of soluble antibodies (Immunocult™ Human CD3/CD28 T Cell Activator) (10971, StemCell), or 10 ng/ml PMA (Phorbol 12-myristate 13-acetate, P8139, Sigma-Aldrich) and 100 ng/ml Ionomycin (I0634, Sigma-Aldrich) or Dynabeads® Human T-Activator CD3/CD28 for T Cell Expansion and Activation (11131D, Thermo Fischer Scientific) (with 1:1 ratio between number of cells and beads) in a 24-well plate for different specified time periods.

RNA extraction

The RNeasy Mini Kit (74106, Qiagen) was employed for RNA extraction following the manufacturer's instructions and including the digestion of genomic DNA with DNAse I (79254, Qiagen). The cells were lysed in RLT buffer (79216, Qiagen), supplemented with 1% beta-Mercaptoethanol (63689, Sigma-Aldrich). NanoDrop 2000c Spectrophotometer (Thermo Fisher Scientific) was used to measure RNA concentration. For the microarray analysis, the quality of RNA was first checked by assessing the RNA integrity number (RIN) using the Agilent RNA 6000 Nano kit (5067-1511, Agilent) and the Agilent 2100 Bioanalyzer Automated Analysis System (Agilent), according to the manufacture's protocol. Only the samples with RIN of 8.5 or higher were used in the further analysis.

Microarray measurement and analysis

The transcriptomic analysis of human effector T cells expanded from CD4+CD25- T cells isolated from the PBMCs of healthy donors were performed on the Affymetrix human gene 2.0 ST array at EMBL Genomics core facilities (Heidelberg, led by Dr. Benes Vladimir). The facility used 500 ng of total RNA in the protocol with the Ambion® WT Expression Kit (cat. 4411974) in order to obtain 10 ug of cRNA, which was then converted to ssDNA. 5.5 ug of ssDNA was labeled and fragmented using the WT Terminal Labeling, polyA and hyb Controls Kit (Affymetrix, cat. 901524). 3.75 ug of fragmented/labeled ssDNA (with hybridization controls) was hybridized to Affymetrix HuGene 2.0 Genechip at 45 °C for 16 hrs with rotation (60 rpm) and washed and stained on GeneChip Fluidics Stations 450 using GeneChip® Hybridization Wash and Stain Kit (Affymetrix, cat. 900720). Arrays were scanned using GeneChip Scanner 3000 7G with GeneChip Command Console software.

The expression signal at the exon level was summarized by the Affymetrix PLIER approach using the sketch approximation of quantile normalization with the option PM-GCBG (a GC content based background correction) using Affymetrix Expression Console v1.3.1.187. Before performing differential analysis, we first pre-processed the data with certain filtering steps. The filtering steps following the PLIER summary method included: 1) first removing any probeset whose cross-hyb type was not equal to 1; 2) removing any probeset corresponding to no identified gene or multiple genes according to the annotation (the file HuGene-2_0-st-v1.na33.2.hg19.transcript) and the library version r4 (May 23, 2012); 3), excluding the probesets with the average expression value in both groups (si_NS and si_VIMP) ≤ 2 times of the median value of the arrays (in our case, 2x the median was equal to the intensity value of 170); 4) if the mean intensity of the probesets in one group was higher, the number of absent calls among the three biological replicates should not be ≥ 1 in the group with higher mean intensity. To secure more robust analysis, we also analyzed the dataset using another model-based method (Berchtold et al., 2008; Weigand et al., 2012), i.e., RMA-sketch summary/normalization method (of note, the filtering steps mentioned above did not apply to the data resulted by the RMA-sketch summary method). We selected the probeset for further analysis only if the two-sided pair-wised T-test generated a P-value lower than 0.05 from the datasets summarized by both PLIER and RMA methods as demonstrated somewhere else (Weigand et al., 2012). To obtain a certain number of starting candidates, we lowered the threshold of the change fold to 1.2, which had to be recurrent in all the three donors, for our further analysis in consideration of both facts that VIMP is not a (co)transcription factor and the siRNA knockdown efficiency was not 100%. The database of mammalian transcription factors or cofactors, or chromatin remodeling factors was downloaded from the work of others (Zhang et al., 2012).

In this way, around 800 genes were significantly upregulated and around 550 genes were downregulated following VIMP knockdown, which were used for further analysis.

Correlation network and IPA

The Teff correlation network based on high-resolution time series datasets of Teffs was already calculated and constructed in our previous work (He et al., 2012) and we extracted the VIMP subnetwork for a deeper analysis in this work. Ingenuity Pathway Analysis (IPA) was used to reconstruct the regulatory network from the Ingenuity database following the instruction of provider (QIAGEN).

cDNA synthesis

The SuperScript™ IV First Strand Synthesis System (18091050, Thermo Fisher Scientific) was used for human cDNA synthesis using a maximum of 500 ng of RNA following the manufacturer's protocol. The master mix for the first step per sample including: 0.5 µl of 50 µM Oligo(dT)20 primers (18418020, Thermo Fisher Scientific), 0.5 µl of 0.09 U/µl Random Primers (48190011, Thermo Fisher Scientific), 1 µl of 10 mM dNTP mix (18427013, Thermo Fisher Scientific) and RNAse free water for a final volume of 13 µl in 0.2 ml PCR Tube Strips (732-0098, Eppendorf). The C1000 Touch Thermal Cycler (Bio-Rad) or UNO96 HPL Thermal Cycler (VWR) were employed with the following program: 5 min at 65 °C, followed by 2 min at 4 °C. For the second reaction step, the reaction mix was accompanied with 40 U RNaseOUT™ Recombinant Ribonuclease Inhibitor (10777019, Thermo Fisher Scientific), 200 U SuperScript™ IV Reverse Transcriptase (18090050, Thermo Fisher Scientific), a final concentration of 5mM Dithiothreitol (DTT) (707265ML, Thermo Fisher Scientific)

and 1x SuperScript™ IV buffer to reach a final reaction volume of 20 µl. We used the following thermocycler program for the second step: 10 min at 50 °C, then 10 min at 80 °C and at 4 °C until further usage. The nuclease-free water was used to dilute the obtained cDNA 5 times with a final volume of 100 µl.

Quantitative real-time PCR

The quantitative real-rime PCR (qPCR) reaction mix per sample enclosed: 5 µl of the LightCycler 480 SYBR Green I Master Mix (04707516001, Roche), 2.5 µl cDNA and 2.5 µl primers in a total reaction volume of 10 ul. The PCR reaction was performed in a LightCycler 480 (384) RT-PCR platform (Roche), using the LightCycler 480 Multiwell 384-well plates (04729749 001, Roche) sealed with the LC 480 Sealing Foil (04729757001, Roche). The program for qPCR used was as follows: 5 min at 95 °C; 45 cycles of (10 sec at 55 °C, 20 sec at 72 °C, 10 sec at 95 °C); melting curve (65-97 °C). The results were analyzed using the LightCycler 480 SW 1.5 software. Primers used for qPCR: RPS9 (QT00233989, Qiagen) as a reference gene, VIMP/SELS (QT00008169, Qiagen), IL2 (QT00015435, Qiagen), CSF2 (QT00000896, Qiagen), IL21 (QT00038612, Qiagen), CEBPG (QT00224357, Qiagen), E2F5 (QT00062965, Qiagen), IRX3 (QT00227934, Qiagen), RNF14 (QT00088291, Qiagen), ZBTB20 (QT00069776, Qiagen) and CTLA4 (QT01670550, Qiagen).

Western blotting

Novex™ WedgeWell 4-20% Tris-Glycine pre-casted gels (XP04202Box, Invitrogen) were used to run and separate proteins in the Novex™ Tris-Glycine SDS Running buffer (LC2675-4, Invitrogen). The proteins were then transferred (dry transfer) using an iBlot2™ Gel Transfer Device (IB21001, Invitrogen) and iBlot2™ PVDF stacks (IB24002, Invitrogen). Following the transfer, the membranes were blocked in 5% milk in PBS with 0.2% Tween20 (PBS-T) for 1 hr at room temperature with gentle shaking and incubated overnight at 4°C together with the primary antibodies, diluted in 5% BSA in PBS-T with 0.025% sodium azide. The next day, the membrane was washed three times (10 min each time) before and after incubation with secondary goat anti-rabbit HRP-coupled antibodies. The Amersham ECL Prime Western Blotting Detection Reagent (RPN2232, GE Healthcare Life Sciences) was used to detect the proteins and the image of the membranes was visualized on the ECL Chemocam Imager (INTAS). If necessary, the contrast and brightness of the obtained whole gel pictures was adjusted using *ImageJ*. The signal intensity of the protein bands was quantified using *ImageJ* and normalized to that of the housekeeping gene GAPDH. For the quantification of phospho proteins, both the phospho and the pan protein were normalized to GAPDH, before normalizing the phospho protein to the total protein.

Target	**Dilution**	**Company**	**Clone**	**Reference**
pNFATC2 (Ser326)	1:100	Sigma-Aldrich		SAB4503945
NFAT1	1:1000	Cell Signaling	D43B1	5861S
VIMP	1:1000	Sigma-Aldrich	Polyclone	V6639
GAPDH	1:200	Santa Cruz Biotechnology	FL-335	SC-25778
Deposited gel data:				
http://dx.doi.org/10.17632/6bd75yg6rp.1				

Proliferation assay

The proliferation of the Teffs was assessed using the CellTrace™ CFSE cell proliferation kit (C34554, Invitrogen). The final concentration of 1 µM CFSE dye was used in our work. To label the cells, they were incubated for exactly 2 min and 45 sec at RT in the dark. To stop the reaction, 10 ml FBS was added and the cells were centrifuged at 200 g for 10 min. After washing the cells in IMDM medium, the cells were subjected to the siRNA knockdown and counted. 10^5 Teff in a 96-well plate were used for each condition and stimulated for 2 days with a ratio of 1:1 of irradiated Epstein Barr Virus (EBV) B cells as previously described (He et al., 2012). After the stimulation, the cells were stained for living cells using LIVE/DEAD® Fixable Near-IR Dead Cell Stain (L10119, Thermo Fisher Scientific) (dilution 1:500) and acquired on a BD Fortessa™ analyzer. The data was analyzed in FlowJo 7.6.5.

Cytokine measurement by Mesoscale discovery (MSD) platform

The cell supernatant was collected after centrifugation of the cells (250 g, 10 min) and the selected list of secreted cytokines (CSF2, IL2, IL21) was measured in the undiluted cell culture medium using the MSD U-PLEX Human Biomarker group 1 kit (MSD, K15067L-1) and following the manufacturer's instructions. MESO QuickPlex SQ 120 instrument was used to read the plate and the data was analyzed with the MSD Workbench software.

Cytokine measurement by Cytometric Bead Array (CBA)

The cell supernatant was collected after centrifugation of the cells and the secreted IL2 in the diluted cell culture medium (1:4 dilution) was measured using the IL2 Flex set cytometric bead array (CBA) (BD, 558270) following the manufacturer's instructions. The acquisition was done on a BD Fortessa™ analyzer and the data was analyzed in FCAP Array™ v3.0.

PhosFlow cytometry analysis

Following stimulation, the cells were immediately fixed by adding the same volume of pre-warmed BD Cytofix Fixation Buffer (554655, BD) for 1 hr at 37 °C. After collecting the samples at all the different time points, they were then washed in FACS buffer and re-suspended in 200 µL of BD Phosflow Perm Buffer III (558050, BD) containing the antibodies for 30 min at 4 °C. After washing the cells with FACS buffer, they were re-suspended in FACS buffer to be acquired on the BD Fortessa™.

The antibodies used are the following (Table below): VIMP/SELS (V6639, Sigma-Aldrich) (dilution 1:200) with Goat Anti-rabbit IgG H&L Alexa Fluor® 647 (A-21245, Invitrogen) (dilution 1:200), NFAT1 FITC (611060, BD) (dilution 1:50), phospho p38 MAPK (T180/Y182) Alexa Fluor 647 (562066, BD) (dilution 1:50), Anti-Human phospho NFATC1 (pS172) mAb (MAB5640, R&D Systems) (dilution 1:400), phospho NFATC2 (NFAT1) (S326) (SAB4503945, Sigma-Aldrich) (dilution 1:800), PE-Cy7 Mouse anti-ERK1/2 (pT202/pY204) (560116, BD) (dilution 1:50), phospho JNK1/2 (T182/Y185) (dilution 1:200) (558268, BD), phospho cJun (S63) (9261S, Cell Signaling) (dilution 1:200), phospho p105 NFκB1 (S933) (4806S, Cell Signaling) (dilution 1:400), phospho p100 NFκB2 (S866/870) (4810S, Cell Signaling) (dilution 1:400), phospho p65 (S529) (558422, BD) (dilution 1:50), phospho RelB (S552) (4999S, Cell Signaling) (dilution 1:400) , Anti-Rabbit IgG H&L Alexa Fluor 647 (ab

150079, Abcam) (dilution 1:1000), APC Goat Anti-mouse IgG (minimal X-reactivity) (405308, Biolegend) (dilution 1:200). For the acquisition a BD Fortessa™ was used and the data was analyzed in FlowJo 7.6.5.

Target	Dilution	Company	Clone (if applicable)	Reference
Anti-VIMP/SELS	1:200	Sigma-Aldrich	Polyclone	V6639
FITC anti-NFATC2 (NFAT1)	1:50	BD Biosciences	1/NFAT-1	611960
Mouse anti-human pNFATC1 (pS172) MAb	1:400	R&D Systems	679340	MAB5640
APC Goat Anti-mouse IgG (minimal X-reactivity) Antibody	1:200	Biolegend	N.A.	405308
Alexa Fluor 647 Mouse anti-NFκB p65 (pS529)	1:50	BD Biosciences	K10-895.12.50	558422
PE-Cy7 Mouse anti-ERK1/2 (pT202/pY204)	1:50	BD Biosciences	20A	560116
Alexa Fluor 647 Mouse Anti-p38 MAPK (pT180/pY182)	1:50	BD Biosciences	36/p38	562066
phospho NFAT1/NFATC2 (S326)	1:800	Sigma-Aldrich	Polyclone	SAB4503945
phospho c-Jun (S63)	1:200	Cell Signaling	Polyclone	9261S
phospho JNK1/2 (T183/Y185)	1:200	BD Biosciences	Polyclone	558268
phospho p105 NFκB1 (S933)	1:400	Cell Signaling	18E6	4806S
phospho p100 NFκB2 (S866/870)	1:400	Cell Signaling	Polyclone	4810S
phospho RelB (S552)	1:400	Cell Signaling	Polyclone	4999S
Goat Anti-rabbit IgG H&L (Alexa Fluor® 647)	1:200	Invitrogen	N.A.	A-21245

Calcium/Ca2+ flux

To measure the calcium flux in Teffs, the cells were stained with mouse monoclonal [RPA-T4] anti-human CD4 FITC (555346, BD Biosciences) (dilution 1:100), LIVE/DEAD® Fixable Near-IR Dead Cell Stain (L10119, Thermo Fisher Scientific) (dilution 1:500) and the calcium dye Indo-1 (I1203, Thermo Fisher Scientific) (5 uM) for 60 min at 37 °C in complete IMDM medium as for the culture of Teffs. Following 3 washes with medium the cells were re-suspended in 300ul of medium and incubated for another 15-30 min at 37°C. The baseline of the calcium signal was measured for approximatively 30 sec before adding the soluble CD3/CD28 antibodies (1:40) (10971, StemCell) or 100 ng/ml Ionomycin (I0634, Sigma-Aldrich) to measure the activation-induced calcium flux. The cells were acquired on a BD Fortessa™ analyzer and the data was analyzed in FlowJo v10.5.

Ethics statement

The study procedures were approved by the ethic committee of the Red Cross Luxembourg. Informed consent was obtained from healthy blood donors through the Red Cross Luxembourg.

Statistical analysis

P values were calculated with paired two-tailed Student t test (Graphpad Prism or Excel) as specified in Figure legend. If the other test was used, it has also been specified in the corresponding Figure legend. All error bars represent the standard deviation.

Supplemental References

Berchtold, N.C., Cribbs, D.H., Coleman, P.D., Rogers, J., Head, E., Kim, R., Beach, T., Miller, C., Troncoso, J., Trojanowski, J.Q., *et al.* (2008). Gene expression changes in the course of normal brain aging are sexually dimorphic. Proc Natl Acad Sci U S A *105*, 15605-15610.

Danileviciute, E., Zeng, N., Capelle, C., Paczia, N., Gillespie, M.A., Kurniawan, H., Coowar, D., Vogt Weisenhorn, D.M., Giro, G.G., Grusdat, M., *et al.* (2019). PARK7/DJ-1 promotes pyruvate dehydrogenase activity and maintains Treg homeostasis. https://doi.org/10.1101/2019.1112.1120.884809.

He, F., Chen, H., Probst-Kepper, M., Geffers, R., Eifes, S., Del Sol, A., Schughart, K., Zeng, A.P., and Balling, R. (2012). PLAU inferred from a correlation network is critical for suppressor function of regulatory T cells. Molecular systems biology *8*, 624.

Probst-Kepper, M., Geffers, R., Kroger, A., Viegas, N., Erck, C., Hecht, H.J., Lunsdorf, H., Roubin, R., Moharregh-Khiabani, D., Wagner, K., *et al.* (2009). GARP: a key receptor controlling FOXP3 in human regulatory T cells. J Cell Mol Med *13*, 3343-3357.

Sawlekar, R., Magni, S., Capelle, C., Baron, A., Zeng, N., Mombaerts, L., Yue, Z., Yuan, Y., He, F.Q., and Gonçalves, J. (2020). Causal dynamical modelling predicts novel regulatory genes of FOXP3 in human regulatory T cells. bioRxiv, 2020.2002.2013.943688.

Weigand, J.E., Boeckel, J.N., Gellert, P., and Dimmeler, S. (2012). Hypoxia-induced alternative splicing in endothelial cells. PLoS One *7*, e42697.

Zhang, H.M., Chen, H., Liu, W., Liu, H., Gong, J., Wang, H., and Guo, A.Y. (2012). AnimalTFDB: a comprehensive animal transcription factor database. Nucleic Acids Res *40*, D144-149.